introducing the 0.1 eV levels into ZnSe in comparable concentrations.

The ZnSe crystals were doped with Al to produce high n-type conductivity samples. Undoped crystals often show high resistivity after heat treatment or irradiation which makes it difficult to perform electrical measurements at low temperatures.

The correlation between irradiation and thermal treatments has also been observed in CdS and CdTe. For example, comparable electron irradiation of an unfired CdTe sample (characterized by curve A of Fig. 1, Ref. 1) produces a crystal showing the same characteristic behavior as a sample fired for 30 min at 900°C in saturated Cd vapor (curve B of Fig. 1, Ref. 1). CdS crystals appear to require much larger irradiation dosages to produce the double acceptor center in similar concentrations.

The defect described in Ref. 1 and this letter appears to be the dominant electrically active defect produced in the n-type II-VI compounds by short metal vapor firing or by electron damage. If other defects are produced, they are either unstable at room temperature or are not electrically active in n-type material. The observation of the described double acceptor center in CdS, CdTe, and ZnSe suggests the general nature of this defect in the II-VI family of compounds.

It has been suggested that a defect of the type reported here may be responsible for part of the edge emission spectra seen in II-VI compounds.[3] However, a relationship between the emission intensity of the optically observed center and the defect concentrations obtained from electrical transport measurements has not yet been established.

The authors acknowledge the aid of B. B. Binkowski, L. H. Esmann, and W. Garwacki in the preparation of the crystals and W. A. Colliton for assistance in the irradiation.

[3] R. E. Halsted and B. Segall, Phys. Rev. Letters **10**, 392 (1963)

PHYSICAL REVIEW VOLUME 132, NUMBER 1 1 OCTOBER 1963

Magnetic Properties of the Hexagonal Antiferromagnet $CsMnF_3$†

KENNETH LEE,* A. M. PORTIS, AND G. L. WITT‡
Department of Physics, University of California, Berkeley, California
(Received 27 May 1963)

The magnetic properties of the hexagonal antiferromagnet $CsMnF_3$ have been investigated by magnetic susceptibility, torsion, electron resonance, and nuclear-antiferromagnetic double resonance. Torsion measurements establish a transition to an antiferromagnetically ordered state at 53.5°K. A weak sixfold anisotropy in the transverse plane and a large axial anisotropy along the c axis corresponding, respectively, to the fields $36K_3/M=1.1$ Oe and $K_1/M=-7500$ Oe are detected. Susceptibility measurements at 4.2°K establish an exchange field $H_E=3.5\times10^5$ Oe. The temperature dependence of K_3 was observed from 4.2°K to the transition temperature and compared with spin-wave and molecular field theory. From paramagnetic resonance measurements an isotropic g value of 1.9989 ± 0.003 is determined. Magnetic resonance measurements below the transition temperature with the applied field in the transverse plane show a weak sixfold anisotropy consistent with the torsion measurements. Measurements out of the transverse plane confirm the large axial anisotropy. In the temperature range from 0.3 to 4.2°K there is an additional temperature dependent anisotropy field $H_{A,T}=9.15/T$ Oe directed along the sublattices. This field arises from the hyperfine interaction with the Mn^{55} nuclear magnetization. Assuming parallel ordering within the transverse planes with adjacent planes alternately magnetized, a calculation of the classical dipolar interactions and of the ligand field anisotropy arising from the displacement of the nearest neighbor fluorines gives a combined axial anisotropy field $K_1/M=-7965$ Oe. The in-plane anisotropy due to second-order dipolar interactions is estimated to be ≈2 Oe in reasonable agreement with observation. The strong coupling between the nuclei and electrons affords an opportunity to observe the Mn^{55} nuclear resonance indirectly by monitoring the position of the electron resonance field. A saturation of the nuclear magnetization is observed at 668 Mc/sec which is $(3\pm1)\%$ smaller than the calculated average hyperfine field of 689 ± 7 Mc/sec. This indicates the presence of a zero-point reduction in the electron spin.

I. INTRODUCTION

SINCE the late 1940's, great strides have been taken in the discovery and experimental observations of antiferromagnetic compounds. In the last few years the compounds $XMnF_3$, where X represents Na, K, and Rb, have been of considerable interest. Like many other double fluorides, these compounds exist in the perovskite-type structure.[1,2] Extensive crystallographic[3–5] and magnetic[6–16] investigations have been

† Supported by the U. S. Atomic Energy Commission.
* Present address: Varian Associates, Palo Alto, California.
‡ National Science Foundation Cooperative Fellow.

[1] R. L. Martin, R. S. Nyholm, and N. C. Stephenson, Chem. Ind. (London) **1956**, 83 (1956).
[2] Yu. P. Simanov, L. R. Batsanova, and L. M. Kovba, Zh.

carried out on $KMnF_3$. This compound is paramagnetic at room temperatures and it becomes a uniaxial antiferromagnet below its Néel Temperature of 88.3°K. However, below 81.5°K the magnetic behavior becomes quite complex; the static magnetic measurements indicated a highly nonlinear magnetic susceptibility.[6,9] This second transition is attributed to an orthorhombic distortion, which causes a canting of the sublattice magnetizations. A weak ferromagnetic moment arising from this canting is therefore responsible for the relatively complex behavior.

The magnetic properties of $RbMnF_3$ have also been studied.[17–20] In contrast to the complex low-temperature behavior of $KMnF_3$, this compound is a simple cubic antiferromagnet below its Néel point of 82°K. The remarkable feature of this compound is that even at low temperatures its crystal structure remains cubic perovskite.

$CsMnF_3$, in contrast to the above compounds, has the same structure as the hexagonal form of $BaTiO_3$.[2,21-23] The dimensions of the hexagonal unit cell are $a=6.213\pm0.003$ Å and $c=15.074\pm0.004$ Å with $c/a=2.426$. With six formula units per cell, the calculated density is 4.84 g/cm³. The space group is $P6_3/mmc$. The atomic coordinates and all the interatomic distances are given in a paper by Zalkin, Lee, and Templeton.[21] A sketch of half of the unit cell is given

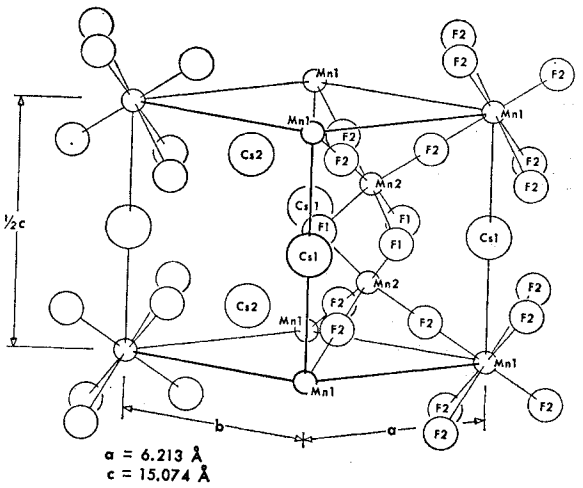

FIG. 1. Sketch of half of the unit cell that shows the two different manganese sites.

in Fig. 1. The structure is built up of six closed-packed layers of Cs and F ions with the Mn ions located in the fluorine octahedral holes between the layers. The Cs_1 atoms have 12 fluorine neighbors arranged as in hexagonal close packing; the point symmetry at these sites is $\bar{6}m2(D_{3h})$. The Cs_2 atoms also have 12 fluorine neighbors, but are arranged as in cubic close packing; the point symmetry at these sites is $3m(C_{3v})$.

The interesting feature of this structure is that there are two manganese sites. One third of the manganese atoms, designated Mn_1, occupy the centers of fluorine octahedra that share their corners with other octahedra, as in the perovskite structure. The remaining two thirds of the manganese atoms, designated Mn_2, are in distorted fluorine octahedra that share one face and three corners with other octahedra. Whereas the point symmetry of the Mn_1 sites is $\bar{3}m(D_{3d})$, the point symmetry about the Mn_2 sites is $3m(C_{3v})$. The Mn_2 atoms are distorted out of their closed packed positions to a distance 3.004 Å apart. The distortion of the structure does not affect greatly the various Mn-F distances, but the various F-F distances range from 2.69 to 3.52 Å.

Consequently, interest arose in the magnetic properties of this compound and the possible effects of the hexagonal structure on its magnetism. A brief account of its magnetic properties was presented earlier.[24] The purpose of this paper is to present a more detailed analysis of the experimental and theoretical magnetic properties. We will first discuss the results of magnetic-susceptibility measurements. Then the results from torsion measurements will be presented. These results obtained at 4.2°K establish that the crystal is ordered antiferromagnetically with a large negative axial anisotropy. Low-field and high-field expressions for the torque will be derived. A discussion of the contri-

Neorgan. Khim. **2**, 2410 (1957); [translation: Russ. J. Inorg. Chem. **2**, 207 (1957)].

[3] A. Okazaki and Y. Suemune, J. Phys. Soc. Japan **16**, 671 (1961).

[4] K. Knox, Acta Cryst. **14**, 583 (1961).

[5] O. Beckman and K. Knox, Phys. Rev. **121**, 376 (1961).

[6] K. Hirakawa, K. Hirakawa, and T. Hashimoto, J. Phys. Soc. Japan **15**, 2063 (1960).

[7] V. Scatturin, L. Corliss, N. Elliott, and J. Hastings, Acta Cryst. **14**, 19 (1961).

[8] O. Beckman, A. J. Heeger, A. M. Portis, and D. T. Teaney, Bull. Am. Phys. Soc. **5**, 188 (1960).

[9] A. J. Heeger, O. Beckman, and A. M. Portis, Phys. Rev. **123**, 1652 (1961).

[10] S. Ogawa, J. Phys. Soc. Japan **15**, 1475 (1960).

[11] A. J. Heeger, thesis, University of California, Berkeley, 1961 (unpublished).

[12] A. J. Heeger, A. M. Portis, D. T. Teaney, and G. Witt, Phys. Rev. Letters **7**, 307 (1961).

[13] W. J. Sandle, Bull. Am. Phys. Soc. **7**, 625 (1962).

[14] G. L. Witt and A. M. Portis, Bull. Am. Phys. Soc. **7**, 625 (1962).

[15] A. J. Heeger, A. M. Portis, and G. Witt, in International Conference on Magnetic and Electric Resonance and Relaxation, Eindhoven, 1962 (unpublished).

[16] A. M. Portis, G. L. Witt, and A. J. Heeger, Suppl. J. Appl. Phys. **34**, 1052 (1963).

[17] D. T. Teaney, J. S. Blackburn, and R. W. H. Stevenson, Bull. Am. Phys. Soc. **7**, 201 (1962); D. T. Teaney, M. J. Freiser, and R. W. H. Stevenson, Phys. Rev. Letters **9**, 212 (1962).

[18] T. R. McGuire, Bull. Am. Phys. Soc. **8**, 55 (1963).

[19] P. E. Seiden, M. J. Freiser, and D. T. Teaney, Bull. Am. Phys. Soc. **8**, 213 (1963); M. J. Freiser, P. E. Seiden, and D. T. Teaney, Phys. Rev. Letters **10**, 293 (1963).

[20] V. L. Morruzzi and D. T. Teaney, Bull. Am. Phys. Soc. **8**, 382 (1963).

[21] A. Zalkin, K. Lee, and D. H. Templeton, J. Chem. Phys. **37**, 697 (1962).

[22] R. D. Burbank and H. T. Evans, Acta Cryst. **1**, 330 (1948).

[23] J. G. Dickinson, L. Katz, and R. Ward, J. Am. Chem. Soc. **83**, 3026 (1961).

[24] K. Lee and A. M. Portis, Bull. Am. Phys. Soc. **7**, 612 (1962).

butions to the anisotropy is included. We will show that the axial anisotropy is due to magnetic dipolar interactions and ligand fields. Finally, we will discuss the dynamical magnetic properties investigated by electron resonance and nuclear-antiferromagnetic double resonance. The macroscopic equations of motion, for both the electrons and the nuclei, will be derived.

II. SUSCEPTIBILITY MEASUREMENTS

Experimental Results

The magnetic susceptibility of $CsMnF_3$ was measured at 298, 77 and 4.2°K using a static force method, the Curie method.[25,26] A small single crystal was placed in a nonhomogeneous magnetic field and the force was measured with a Faraday balance. The sample is mounted in a cylindrically shaped Teflon cradle which in turn is connected via a 1.5-mm o.d. quartz tube to a 0.002-in. beryllium-copper wire. This wire is then attached to one arm of the balance. The Teflon cradle has a removable cap on which the sample is mounted. The apparatus was calibrated with a MnF_2 single crystal.

From torsion measurements (next section) a transition to an ordered state was observed at 53.5°K. The susceptibility measurements at 4.2°K were, therefore, made parallel and perpendicular to the symmetry axis, the c axis. The values of the susceptibilities at the different temperatures are $\chi(298°K)=10.6\times10^{-3}$ emu/mole, $\chi(77°K)=27.9\times10^{-3}$ emu/mole, and $\chi(4.2°K)=39.7\times10^{-3}$ emu/mole, where $\chi(4.2°K)$ represents the average susceptibility determined with the field parallel and perpendicular to the c axis. The 4.2°K results were obtained for fields of 3.8 to 5.3 kOe. The values obtained in the paramagnetic region are consistent with the values obtained by Teaney.[27]

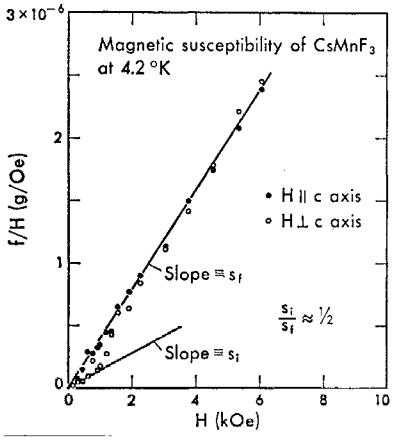

FIG. 2. Force divided by magnetic field versus magnetic field at 4.2°K. The force is in gram units.

[25] T. R. McGuire, in *Solid State Physics*, edited by K. Lark-Horovitz and V. A. Johnson (Academic Press Inc., New York, 1959), Vol. 6, p. 171. T. R. McGuire and C. T. Lane, Rev. Sci. Instr. 20, 489 (1949).
[26] G. K. White, *Experimental Techniques in Low Temperature Physics* (Oxford University Press, New York, 1959).
[27] D. T. Teaney (private communication).

A graph of f/H as a function of H in the ordered state is shown in Fig. 2. All the data, within experimental error, lie on a straight line and extrapolate to zero. Below 1 kOe, the slope of the data taken perpendicular to the c axis is approximately $\frac{1}{2}$ of the slope for larger applied fields; it is also approximately $\frac{1}{2}$ of the slope of the data taken parallel to the c axis.

No hysteresis was observed parallel to the c axis. Hysteresis perpendicular to the c axis was not observable because of the free rotational suspension of the sample.

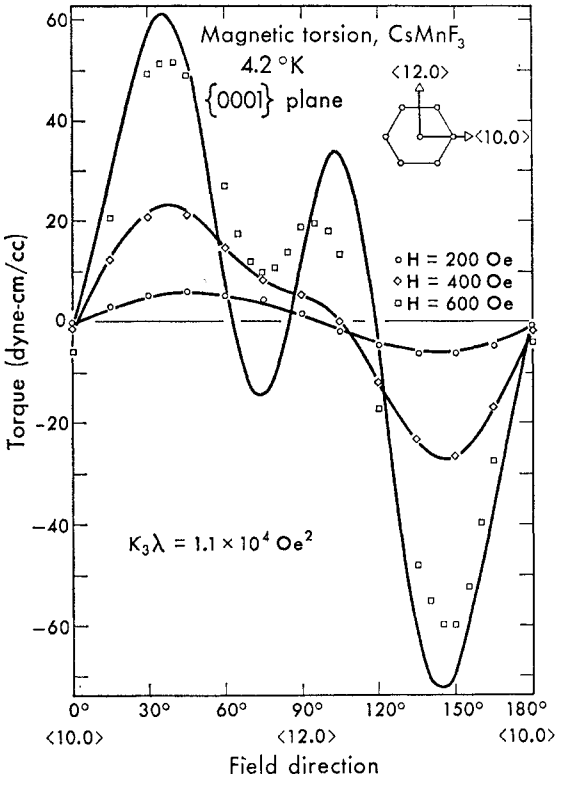

FIG. 3. Low field magnetic torsion measurements in the {0001} plane at 4.2°K. The theoretical curves are given by the low-field expression for the torque. Note the emergence of sixfold symmetry with increasing field.

Interpretation of Results

Since we did not observe any hysteresis or a nonzero extrapolation in the f/H versus H graph, we conclude that this compound is neither a ferromagnet nor a canted antiferromagnet with a weak ferromagnetic moment parallel to the c axis. All the measurements indicate an antiferromagnetic ordering.

The fact that the slope of the f/H versus H graph, for H in the transverse plane, is approximately $\frac{1}{2}$ of the final slope, indicates the sublattice magnetizations lie parallel to the plane. This factor of $\frac{1}{2}$ arises from the absence of a contribution of the parallel susceptibility to the total susceptibility. If the magnetizations are

parallel to the plane, it is not unreasonable to assume that since there is sixfold symmetry in the plane, there will be domains of magnetization along three equivalent easy directions in the plane. As long as the applied field is below the critical field for flopping ($H_c \sim 10^3$ Oe) the total measured susceptibility would include a parallel contribution according to the relation

$$\langle\chi\rangle_{av}=\tfrac{1}{2}\chi_\perp+\tfrac{1}{2}\chi_{\parallel},$$

where $\chi_\perp$ and $\chi_{\parallel}$ are, respectively, the susceptibilities perpendicular and parallel to the magnetizations. At 4.2°K, $\chi_{\parallel}$ is nearly zero so that the average susceptibility is smaller than the perpendicular susceptibility by a factor of $\frac{1}{2}$.

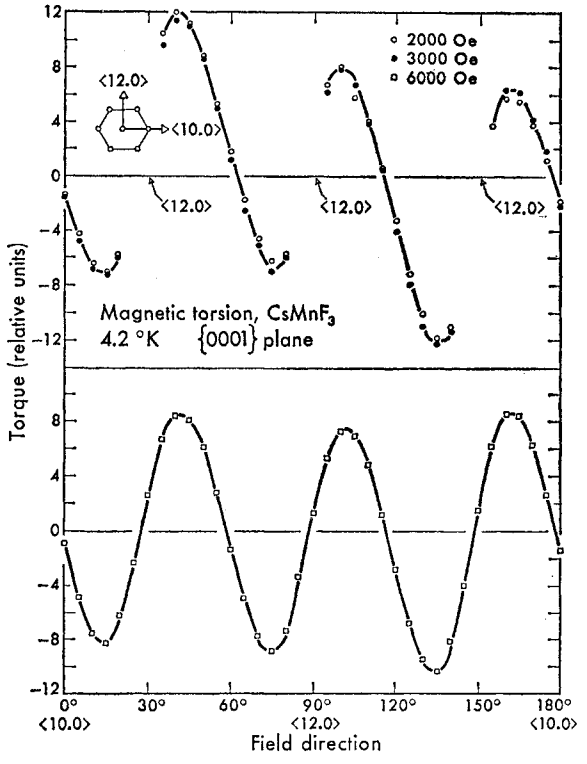

FIG. 4. Intermediate- and high-field magnetic torsion measurements in the {0001} plane at 4.2°K. For fields up to 5 kOe, discontinuities occur along the ⟨12.0⟩ directions and for fields greater than or equal to 6 kOe, a pure sixfold dependence is observed. Note the torque at high fields is independent of the field.

For fields much larger than H_c, the susceptibility is observed to be larger in the transverse plane. This is also an indication that the magnetizations lie in the plane.

III. TORSION MEASUREMENTS

Experimental Results

The anisotropy of a single crystal of $CsMnF_3$ was investigated by torsion measurements in a uniform field from 4.2 to 77°K. The apparatus is quite similar to that

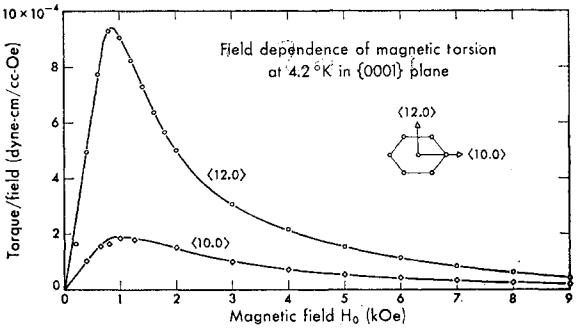

FIG. 5. Field dependence of magnetic torsion in the {0001} plane at 4.2°K. This is a plot of the torque divided by the field versus the field. At low fields, the torque is proportional to H^2.

used by Stout and Griffel[28] and Heeger.[9] The crystal is mounted to the same Teflon cradle and quartz rod used in the susceptibility measurements and the beryllium-copper wire is attached to a rotating torsion head. A mirror, attached to the rod, determines the orientation of the sample with respect to a zero-field position. The torque is then determined by rotating the torsion head back to this position. To measure the torque as a function of temperature, a heater was wound around the copper can containing the freely suspended sample. A copper-constantan thermocouple, with a reference temperature of 77°K, was used to measure the temperature. Except for the measurements of the torque as a function of temperature, all the measurements were carried out at 4.2°K. The sample weighed 20.5 mg.

Low-field torsion measurements in the transverse plane are shown in Fig. 3. The theoretical curves are also shown. At very low fields a $\sin 2\varphi$ dependence predominates. With slightly greater field, a $\sin 4\varphi$ dependence is observed, and finally a sixfold dependence emerges for greater applied fields.

For intermediate and high fields, the angular dependence of the torque is shown in Fig. 4. For applied fields up to 5 kOe, discontinuities were observed along the ⟨12.0⟩ directions, suggesting that the sublattice magnetizations are along these directions in zero field. For fields greater than or equal to 6 kOe, the discontinuities vanish, giving rise to a pure sixfold dependence. This indicates that the magnetizations are being freely pulled around by the applied field. Zero torque is always observed when the field is along the ⟨12.0⟩ and ⟨10.0⟩ directions. These two plots indicate the ⟨12.0⟩ directions correspond to minimum energy orientations and the ⟨10.0⟩ directions correspond to maximum energy orientations.

The field dependence of the torque in the transverse or {0001} plane is shown in Fig. 5. This is a plot of the torque divided by the field versus the field applied along the two principal directions in the plane. The torque divided by field is just the net moment perpendicular to the applied field. For fields up to 600 Oe, the

[28] J. W. Stout and M. Griffel, J. Chem. Phys. 18, 1449 (1950).

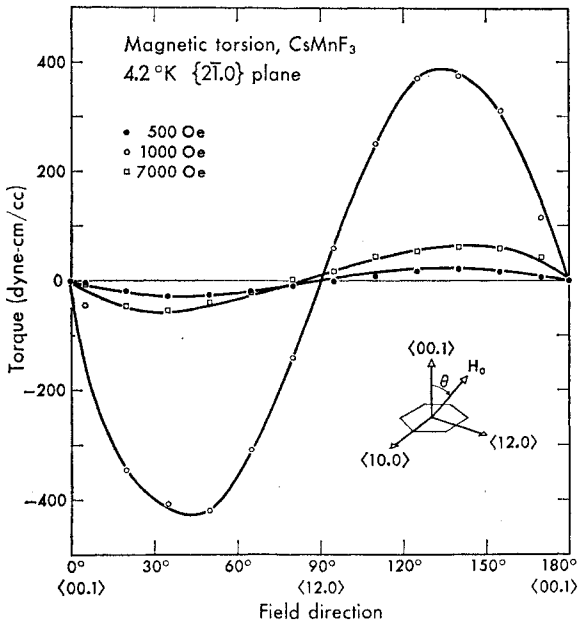

FIG. 6. Magnetic torsion in the {2$\bar{1}$.0} plane at 4.2°K. The torque is zero with the field along the ⟨00.1⟩ and ⟨12.0⟩ directions.

torque along the two directions is proportional to H^2. This indicates the absence of a weak ferromagnetic moment in the plane. Upon attaining a maximum at approximately 900 Oe, the torque decreases to a constant value above 9 kOe. Coupled with the observations of sixfold symmetry for fields greater than or equal to 900 Oe, a critical field H_c of about 900 Oe is indicated. No hysteresis was observed with the field parallel or perpendicular to the transverse plane.

The angular dependence of the torque was also observed in the {2$\bar{1}$.0} plane. This is shown in Fig. 6 for fields up to 7 kOe. The torque is zero with the field along the ⟨00.1⟩ and ⟨12.0⟩ directions. The torque for applied fields of 500 and 7 kOe have a period of 180°. The torque at the intermediate field, 1 kOe, has in addition a small $\sin 4\theta$ dependence. These measurements reveal the presence of a large negative axial anisotropy. The transverse plane is, therefore, an 'easy' plane. The torque has twofold symmetry in this plane because of the uniaxial symmetry of the c axis. The presence of the small fourfold dependence for an applied field of 1 kOe is due to the flopping of the magnetizations in the plane.

Finally, the temperature dependence of the torque parallel and perpendicular to the transverse plane with fields from 800 Oe to 7kOe was observed. No torque was observed above 53.5°K. Since the torque in the transverse plane at high fields has sixfold symmetry, one would expect the torque to be directly proportional to the sixfold anisotropy energy, K_3. And in fact, it will be shown in the next section that for fields much greater than the critical field for flopping, the torque is given by

$$\tau = -12K_3 \sin 6\varphi_0,$$

where φ_0 is the position of the applied field H_0 with respect to a ⟨12.0⟩ direction. Figure 7 shows the temperature dependence of the torque, i.e., the sixfold anisotropy energy. A field of 6 kOe was applied along a direction 45° with respect to a ⟨12.0⟩ direction.

From these torsions measurements, we have found (1) no evidence of either a weak ferromagnetic moment in the transverse plane or a screw structure, (2) a weak sixfold anisotropy in the plane, (3) an antiferromagnetic ordering with a large negative axial anisotropy, (4) a critical field of 900 Oe, (5) the ⟨12.0⟩ and ⟨10.0⟩ correspond, respectively, to the easy and hard directions, and (6) a transition at 53.5°K to the disordered state. These measurements are consistent with the susceptibility measurements.

At low fields, the magnetic moments may be in six equivalent directions in the transverse plane. If all six equivalent domains were equally present, there should be sixfold symmetry in the torque at all fields. However, because there are deviations, we conclude that there exists at low fields inequivalent population of spins along the six directions.

Theory of Torsion and Anisotropy

In this section we derive low- and high-field expressions for the torque. We then discuss the temperature dependence of sixfold anisotropy energy. Finally, we calculate the magnetic dipolar and ligand field contributions to the anisotropy. We will show that the ligand fields due to the distortion of the fluorine octahedra and the classical magnetic dipolar interactions give rise to a large negative axial anisotropy consistent with experimental observations. Although no specific calculations are carried out for the sixfold anisotropy, we will show it not to be unlikely that this anisotropy arises from second-order dipolar interactions.

In deriving the theoretical expressions for the torque (and in a later section the expressions for the electron and nuclear resonance) we assume a two sublattice

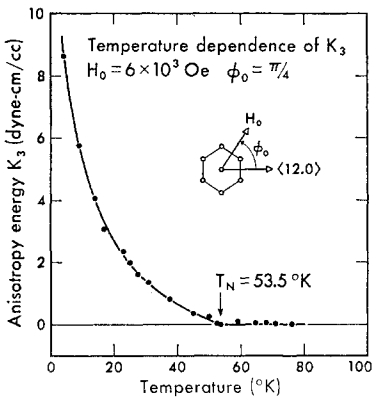

FIG. 7. Temperature dependence of the sixfold anisotropy energy. A field of 6 kOe is applied at 45° with respect to a ⟨12.0⟩ direction. A Néel temperature of 53.5°K is observed.

model consistent with experimental observations. That is, we assume the magnetizations to lie in the transverse plane along the ⟨12.0⟩ directions with a negative axial anisotropy energy $K_1\cos^2\theta$. The sixfold anisotropy energy in the plane is given by $K_3\sin^6\theta\cos 6\varphi$.[29] With the angles defined in Fig. 8, we have for the total energy

$$U=-(\mathbf{M}_1+\mathbf{M}_2)\cdot\mathbf{H}_0+\lambda\mathbf{M}_1\cdot\mathbf{M}_2 -K_3(\sin^6\theta_1\cos 6\varphi_1+\sin^6\theta_2\cos 6\varphi_2) +\tfrac{1}{2}K_1(\cos^2\theta_1+\cos^2\theta_2), \quad (1)$$

where $K_1>0$ and $K_3>0$.

Low-Field Theory

We proceed to derive an expression for the torque in the transverse plane for low fields. By low fields, we mean fields smaller than the critical field H_c. We assume unequal spin populations along the six equivalent directions in the transverse plane. We let $\theta_0=\theta_1=\theta_2=\frac{1}{2}\pi$. We initially concern ourselves with one of the six equivalent directions. The energy is

$$U=-K_3(\cos 6\varphi_1+\cos 6\varphi_2)-\lambda M^2\cos(\varphi_1+\varphi_2) +MH_0[\cos(\varphi_0+\varphi_2)-\cos(\varphi_0-\varphi_1)]. \quad (2)$$

The torque is then given by

$$\tau=MH_0[\sin(\varphi_0-\varphi_1)-\sin(\varphi_0+\varphi_2)]. \quad (3)$$

Now we introduce the new parameters Φ and Δ:

$$\Phi=\tfrac{1}{2}(\varphi_1-\varphi_2+\pi), \qquad \Delta=\tfrac{1}{2}(\varphi_1+\varphi_2), \quad (4)$$

where Δ is small. The sublattice magnetizations are induced by the applied field to cant slightly away from the easy directions. The amount of canting is given by Δ and the position of the net moment due to the canting is given by Φ. Rewriting the energy and torque expressions in terms of the new parameters, we have

$$U=-2K_3(1-18\Delta^2)\cos 6\Phi-\lambda M^2(1-2\Delta^2) -2MH_0\Delta\cos(\varphi_0-\Phi), \quad (5)$$

$$\tau=(H_0^2/2\lambda)\sin 2(\varphi_0-\Phi). \quad (6)$$

The equilibrium position is then given by

$$\Delta=\frac{H_0\cos(\varphi_0-\Phi)}{2H_E+H_{A,3}\cos 6\Phi}\approx\frac{H_0\cos(\varphi_0-\Phi)}{2H_E}, \quad (7)$$

where $H_E=\lambda M$ and $H_{A,3}=36K_3/M$. We assume $H_E\gg H_{A,3}$, which is quite valid from experimental observations. Substituting Eq. (7) into Eq. (5) gives an expression of the energy as a function of φ_0 and Φ. Now we solve for Φ in terms of φ_0 by taking $\partial U/\partial\Phi=0$ and expanding in powers of the applied field to order

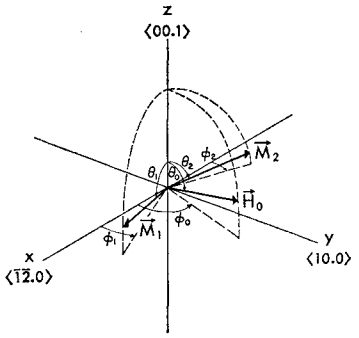

FIG. 8. Definition of the angles used. The z axis coincides with the ⟨00.1⟩ direction. The x and y axes are parallel, respectively, to the ⟨1̄2.0⟩ and ⟨10.0⟩ directions.

H_0^6. We find

$$\sin 2\Phi\simeq-(H_0^2/72K_3\lambda)\sin 2\varphi_0 -(H_0^2/72K_3\lambda)^2\sin 2\varphi_0\cos 2\varphi_0. \quad (8)$$

Substituting into Eq. (6) we have

$$\tau=(H_0^2/2\lambda)\{[1-\tfrac{1}{8}(H_0^2/72K_3\lambda)^2]\sin 2\varphi_0 +\tfrac{1}{2}(H_0^2/72K_3\lambda)\sin 4\varphi_0 +\tfrac{3}{8}(H_0^2/72K_3\lambda)^2\sin 6\varphi_0\}. \quad (9)$$

Now we take into account that there are six equivalent directions with unequal spin populations. Let a_0, a_1, and a_2 represent the fraction of the total spins along the six directions such that

$$a_0(+,-)+a_1(+,-)+a_2(+,-)=1. \quad (10)$$

Because the parameter is given by $\Phi=\Phi(H_0)$ we assume a small change in Φ due to the angular variation of the small applied field H_0. Since

$$\Phi_{H=0}=0,\ \pi/3,\ 2\pi/3,\ \cdots, \quad (11)$$

which follows from the definition of Φ, we have

$$\Phi=(n\pi/3)+\delta, \quad n=0,1,2. \quad (12)$$

To lowest order in H_0, i.e., $H_0\ll H_c$, $\delta\simeq 0$ and

$$\tau=(H_0^2/2\lambda)\sin 2(\varphi_0-n\pi/3)$$

is the torque due only to the spins along the nth direction. Therefore, to $O(H_0^6)$, the total torque due to the spins along the six directions is

$$\tau=\sum_{n=0}^{2}a_n\frac{H_0^2}{2\lambda}\left\{\left[1-\frac{1}{8}\left(\frac{H_0^2}{72K_3\lambda}\right)^2\right]\sin 2(\varphi_0-n\pi/3) +\frac{1}{2}\left(\frac{H_0^2}{72K_3\lambda}\right)\sin 4(\varphi_0-n\pi/3) +\frac{3}{8}\left(\frac{H_0^2}{72K_3\lambda}\right)^2\sin 6(\varphi_0-n\pi/3)\right\}. \quad (13)$$

Carrying out the sum and defining a phase factor ζ given by

$$\tan 2\zeta=\tfrac{1}{2}\sqrt{3}(a_0-a_2)/(\tfrac{1}{2}(a_0+a_2)-a_1) \quad (14)$$

[29] H. S. Belson and C. J. Kriessman, Suppl. J. Appl. Phys. **30**, 175 (1959). J. Smit and H. P. J. Wijn, *Ferrites* (John Wiley & Sons, Inc., New York, 1959).

and a constant

$$D=(\tfrac{1}{2}(a_0+a_2)-a_1)/\cos 2\varphi_0 \tag{15}$$

we have finally,

$$\tau=(H_0^2/2\lambda)[1-\tfrac{1}{8}(H_0^2/72K_3\lambda)^2]D\sin 2(\varphi_0-\zeta)$$
$$+18K_3\left(\frac{H_0^2}{72K_3\lambda}\right)^2 D\sin 4\left(\varphi_0+\frac{\zeta}{2}\right)$$
$$-\frac{27}{2}K_3\left(\frac{H_0^2}{72K_3\lambda}\right)^3\sin 6\varphi_0. \tag{16}$$

We note that to lowest order in H_0, $\tau\sim H_0^2$. Also if the spin populations are equal D and ζ vanish, leaving only a sixfold dependence of the torque, which is as expected. Our assumption that the $\langle 12.0\rangle$ directions correspond to the easy directions in the plane is consistent with experimental observations.

High-Field Theory

We derive expressions for the torque with H_0 in the $\{2\bar{1}.0\}$ plane and in the transverse plane. We assume $H_0\gg H_c$ and $H_0\gg H_{A,3}$. In this case, we expect the magnetizations to flop into a perpendicular orientation with respect to the field. Let us first discuss the case where H_0 is in the transverse plane. As the field is rotated in the plane, the magnetizations follow, always oriented approximately perpendicular to H_0. That is, the angles are given by

$$\varphi_0\mp\varphi_{1,2}=\tfrac{1}{2}\pi. \tag{17}$$

We let $\varphi_{1,2}=\pm\varphi+\epsilon$ where the small amount of canting toward the field is given by ϵ. The energy is given by Eq. (1) and the equilibrium conditions are obtained by setting

$$\partial U/\partial\varphi_1=\partial U/\partial\varphi_2=0 \quad \text{with} \quad \theta_1=\theta_2=\tfrac{1}{2}\pi.$$

In terms of the new parameters, the conditions are

$$\begin{aligned} 6K_3\sin 6(\varphi+\epsilon)+\lambda M^2\sin 2\epsilon &= MH_0\sin(\varphi_0-\varphi-\epsilon), \\ 6K_3\sin 6(-\varphi+\epsilon)+\lambda M^2\sin 2\epsilon &= MH_0\sin(\varphi_0-\varphi+\epsilon). \end{aligned} \tag{18}$$

Expanding to first order in ϵ and assuming strong exchange coupling $H_E\gg H_{A,3}$ and $H_E\gg H_0$, we find

$$\epsilon\simeq H_0\sin(\varphi_0-\varphi)/2H_E \tag{19}$$

and

$$24K_3\lambda\sin 6\varphi=H_0^2\sin 2(\varphi-\varphi_0). \tag{20}$$

Solving this expression graphically, we find $\varphi_0-\varphi=\frac{1}{2}\pi$ which is what we expect for stable equilibrium. In the limit of $H_0\gg H_c$, we let $\varphi_0-\varphi=\frac{1}{2}\pi-\zeta$ where ζ is a small deviation from $\frac{1}{2}\pi$. Substituting into Eq. (20), we find

$$\zeta=(12K_3\lambda/H_0^2)\sin 6\varphi_0. \tag{21}$$

Therefore the equilibrium orientations are given by

$$\varphi_{1,2}=\pm[\varphi_0-\tfrac{1}{2}\pi+\zeta]+\epsilon \tag{22}$$

where from Eq. (19)

$$\epsilon=(H_0/2H_E)\cos\zeta. \tag{23}$$

From Eq. (3), we have for the torque

$$\tau=-2MH_0\sin\zeta\sin\epsilon. \tag{24}$$

In the limit of ζ and ϵ small and $H_0^2>\frac{1}{3}H_{A,3}H_E$ the torque is

$$\tau=-12K_3\sin 6\varphi_0. \tag{25}$$

We now consider the case with the field in the $\{2\bar{1}.0\}$ plane. With H_0 along the $\langle 12.0\rangle$ and $\langle 00.1\rangle$ directions, we determine the equilibrium positions and find for H_0 parallel to the $\langle 12.0\rangle$ direction,

$$m_b=2MH_0/(2H_E+H_{A,3}) \tag{26}$$

and for H_0 parallel to the $\langle 00.1\rangle$ direction

$$m_c=2MH_0/(2H_E+H_{A,1}) \tag{27}$$

where $H_{A,1}=K_1/M$ and m_b and m_c are the induced moments along the two respective directions. With H_0 at an angle θ_0 with respect to the c axis, the energy is

$$U=-MH_0^2\left[\frac{2\sin^2\theta_0}{2H_E+H_{A,3}}+\frac{2\cos^2\theta_0}{2H_E+H_{A,1}}\right]. \tag{28}$$

Expanding in terms of $H_{A,3}/H_E$ and $H_{A,1}/H_E$ and neglecting $H_{A,3}$ with respect to $H_{A,1}$, we find the following expression for the torque:

$$\tau=-\frac{MH_0^2}{2H_E^2}H_{A,1}\sin 2\theta_0. \tag{29}$$

We note that Eqs. (26) and (27) also determine the susceptibility parallel and perpendicular to the c axis. With $H_{A,3}\ll H_E$, we have

$$(\chi_b-\chi_c)/\chi_b=1-2H_E/(2H_E+H_{A,1}). \tag{30}$$

Therefore, if $H_{A,1}\sim 10^4$ and $H_E\sim 10^6$, the difference in the susceptibilities is of the order of 1%.

Temperature Dependence of Anisotropy Energy

The temperature dependence of the anisotropy energies in antiferromagnets is fairly well understood theoretically in two limiting temperature regions. The two regions are the region at very low temperatures where spin-wave theory is appropriate and the region at very high temperatures where the Weiss molecular field theory is appropriate. In this section, we will review the basic results in these two regions.

At low temperatures Pincus[30] used spin-wave calcu-

[30] P. Pincus, Phys. Rev. **113**, 769 (1959).

lations to derive the following relation

$$K(T)/K(0)=[M(T)/M(0)]^{\frac{1}{2}n(n+1)}, \qquad (31)$$

where $K(T)$ is the anisotropy constant corresponding to the nth order surface harmonic, $M(T)$ refers to the sublattice magnetization and $K(0)$ and $M(0)$ refer to the corresponding quantities at absolute zero. This relation is only valid over a temperature range such that $\Delta M/M(0)\ll 1$. Short-range interactions are assumed such that this derivation does not apply to the dipolar (long-range) contributions to the anisotropy. Zero-point fluctuation[31] is also included. This result is analogous to the Abulov-Zener[32] result for the short-range interaction contribution to the anisotropy energy in ferromagnets.

Calculations of $M(T)/M(0)$ at low temperature have been made by Anderson,[31] Kubo,[33] and Eisele and Keffer[34] using spin-wave theory. The result is[35]

$$\frac{\Delta M}{M(0)}=\frac{1}{S}P\left(\frac{\pi^2}{6}\right)\left(1+\frac{H_{A,1}}{H_E}\right)\left[\frac{1}{3}(S+1)\frac{T}{T_N}\right]^2 \times m\left(\frac{T}{T_H}\frac{T}{T_{AE}}\right), \qquad (32)$$

where the lattice factor for cubic lattices of dimension a is

$$P=(3^{3/2}/\pi^2)(\tfrac{1}{2}Na^3)=(\tfrac{1}{2}\pi^2)(\tfrac{1}{2}Z)^{3/2}$$

and

$$m\left(\frac{T}{T_H}\frac{T}{T_{AE}}\right)=\frac{6}{\pi^2}\frac{T_{AE}}{T}\sum_{P=1}^{\infty}\frac{1}{P}K_1\left(P\frac{T_{AE}}{T}\right)\cos\left(P\frac{T_H}{T}\right).$$

K_1 is the Hankel function, S is the total spin, Z is the number of nearest neighbors, H_E and H_A are the exchange and anisotropy energies, $\frac{1}{2}N$ is the number of magnetic ions for each sublattice,

$$kT_H=g\mu_B H_0[1-(\chi_{11}/2\chi_\perp)],$$

and $T_{AE}=(\hbar\gamma/k)[2H_AH_E+H_A^2]^{1/2}$ is the temperature corresponding to the gap in the spin-wave spectrum for an antiferromagnet.

The quantity $m(T/T_H,T/T_{AE})$ takes into account the suppression of spin-wave excitation because of the energy gap and it approaches unity for $T/T_{AE}\gg 1$.

According to the molecular field theory in the high-temperature region, the anisotropy energy is proportional to the square of the spontaneous magnetization of each sublattice where the spontaneous sublattice magnetization is given by the Brillouin function,

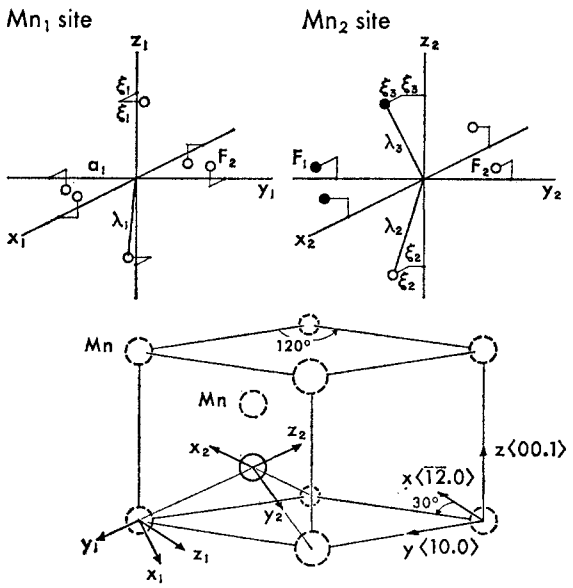

FIG. 9. Fluorine distortions in $CsMnF_3$. The coordinate systems at each Mn^{2+} site, the general coordinate system and their relative orientation to each other in the unit cell are shown.

$B_s(Y)$.[36,37] That is,

$$M(T)=\tfrac{1}{2}Ng\mu_B SB_s(Y), \qquad (33)$$

where $y=(g\mu_B SH_{\text{eff}}/kT)$.

Ligand Field Anisotropy

We now consider the anisotropy energy arising from the ligand field acting on each of the two Mn^{2+} sites (Fig. 1). This energy can be expressed as a function of the spin of the Mn^{2+} ion. In order to calculate the symmetry of the ligand field, we regard the surrounding F^- ions as point sources. The fluorine displacements about the Mn_1 and Mn_2 sites are shown in Fig. 9.[38] Also shown are the individual coordinate systems and the general coordinate system (x,y,z). The magnitudes of the displacements are determined from the x-ray analysis[21] with the point symmetry about each site preserved. The Mn_1 sites are surrounded by a distorted octahedron of F_2 sites which are displaced by ξ_1, while the Mn_2 sites are surrounded by three F_2 and three F_1 sites which are respectively displaced by ξ_2 and ξ_3. The fluorine displacements and distances to the Mn^{2+}

[31] P. W. Anderson, Phys. Rev. **86**, 694 (1952).
[32] N. Akulov, Z. Physik **100**, 197 (1936); C. Zener, Phys. Rev. **96**, 1335 (1954).
[33] R. Kubo, Phys. Rev. **87**, 568 (1952).
[34] J. A. Eisele and F. Keffer, Phys. Rev. **96**, 929 (1954).
[35] F. Keffer (to be published).
[36] T. Nagamiya, K. Yosida, and R. Kubo, Advan. Phys. **4** (1955).
[37] It is noted that T. Nakamura [Phys. Rev. **128**, 2500 (1962)] has studied the temperature dependence of the magnetic anisotropy with tetragonal symmetry for an antiferromagnet near the Néel point. He finds the magnetic anisotropy to have a singularity of order $(T-T_N)^{-1/2}$.
[38] Because of the relatively low symmetry ($P6_3/mmc$) of the structure at room temperature, the lattice distances and space group, to a good approximation, are the same at low temperatures. In all our discussions, we will assume the same crystal structure at all temperatures.

sites are

$$\begin{aligned}
&\text{Mn}_1 \text{ site}, \quad \xi_1=0.0262a_1,\\
&\qquad\qquad a_1=2.1185\ \text{Å},\\
&\qquad\qquad \lambda_1=2.12\ \text{Å};\\
&\text{Mn}_2 \text{ site}, \quad \xi_2=0.044a_2,\\
&\qquad\qquad \xi_3=0.1117a_2,\\
&\qquad\qquad a_2=2.118\ \text{Å},\\
&\qquad\qquad \lambda_2=2.12\ \text{Å},\\
&\qquad\qquad \lambda_3=2.144\ \text{Å}.
\end{aligned}$$

Note that ξ_3 is four times larger than ξ_1.

The potential in the region of each of the Mn^{2+} sites as a function of the fluorine displacements is first determined in the respective coordinate systems.[39] The potentials about the Mn_1 and Mn_2 sites are written to fourth order in the distances from the site and to first and second order, respectively, in the lattice distortions ξ_1 and $\xi_{2,3}$. A transformation to a set of crystal axes is then carried out. Since the single ion anisotropy energy transforms in the same way as the potential, it can be immediately written as an expansion in powers of the spin components. The magnetic energy per unit volume is then written in terms of the sublattice magnetizations $\mathbf{M}_{1,2}=\frac{1}{2}Ng\mu_B\mathbf{S}_{1,2}$. Finally, in terms of the polar coordinates, the magnetic energy per unit volume for the Mn_1 site is

$$U^{(1)}=K_1^{(1)}\sin^2\theta_1+K_2^{(1)}\sin^4\theta_1 +K_2^{(1)\prime}\sin^2\theta_1\sin 2\theta_1\cos 3\varphi_1 \quad (34)$$

and for the Mn_2 site is

$$U^{(2)}=K_1^{(2)}\sin^2\theta_2+K_2^{(2)}\sin^4\theta_2 -K_2^{(2)\prime}\sin^2\theta_2\sin 2\theta_2\cos 3\varphi_2 \quad (35)$$

where $K_1^{(1)}$, $K_2^{(1)}$ and $K_2^{(1)\prime}$ are proportional to $-\xi_1$ and $K_1^{(2)}$, $K_2^{(2)}$, and $K_2^{(2)\prime}$ are proportional to $-(\xi_3-\xi_2)$ and $-(\xi_3^2+\xi_2^2)$. The angles are defined in Fig. 8. Since all the coefficients are negative, we see that the crystalline fields arising from the distortion of the nearest neighbor fluorine octahedrons give rise to a negative axial anisotropy. That is, the transverse plane is an easy plane.

To obtain an estimate of the anisotropy, the potentials to lowest order are given by

$$\begin{aligned}
&\Phi^{(1)}=\tfrac{1}{2}D_1\xi_1[2S_z^2-(S_x^2+S_y^2)],\\
&\Phi^{(2)}=\tfrac{1}{2}D_2\left[(\xi_3-\xi_2)+\frac{1}{2a_2}(\xi_3^2+\xi_2^2)\right] \times[2S_z^2-(S_x^2+S_y^2)],
\end{aligned} \quad (36)$$

where $D_2=\frac{1}{4}D_1$.[39] The energy is therefore of the form $-(\frac{1}{2}K_c)(3\cos^2\theta-1)$. Assuming a small displacement $\delta\theta$ out of the transverse plane, $U\sim\frac{3}{2}K_c(\delta\theta)^2=\frac{1}{2}MH_A^{\text{eff}}(\delta\theta)^2$, and therefore, the effective anisotropy field $H_A^{\text{eff}}=-3K_c/M$.

Now the single-ion anisotropy energy determined earlier by torsion measurements in $KMnF_3$ is equal to

$$D_1\epsilon=-2K_c/NS^2=-9.6\times10^{-18}\ \text{ergs/ion},$$

where $\epsilon=0.035$ is a unit of strain in this lattice.[9] The effective anisotropy field per unit strain is thus given by

$$H_A^{\text{eff}}=3D_1S/g\mu_B=10.9\times10^4\ \text{Oe}. \quad (37)$$

From Eqs. (36), we see that the single-ion anisotropy energies for the Mn_1 and Mn_2 sites are proportional to ξ_1, and

$$\tfrac{1}{4}[(\xi_3-\xi_2)+(1/(2a_2))(\xi_3^2+\xi_2^2)].$$

The effective anisotropy fields due to the two sites are then determined to be

$$H_A^{\text{eff}}(\text{Mn}_1)=\frac{\xi_1}{a(\text{KMnF}_3)}(10.9\times10^4)=1450\ \text{Oe}$$

and

$$H_A^{\text{eff}}(\text{Mn}_2)=\frac{[(\xi_3-\xi_2)+(1/(2a_2))(\xi_3^2+\xi_2^2)]}{4a(\text{KMnF}_3)} \times(10.9\times10^4)=1035\ \text{Oe},$$

where $a(KMnF_3)=4.172$ Å. Since there are twice as many Mn_2 sites as there are Mn_1 sites, the average effective axial anisotropy field is

$$H_A^{\text{eff}}(\text{crystal})=1170\ \text{Oe}. \quad (38)$$

Dipolar Anisotropy

The anisotropy due to classical dipolar interactions will now be determined. From the hexagonal symmetry of the structure, it is obvious that classical interactions will not give rise to any anisotropy in the transverse plane. This is because the dipole-dipole term in the Hamiltonian $\mathcal{H}_D$ is only quadratic in the direction cosines, whereas the term in the anisotropy energy describing the sixfold symmetry is written to the sixth power in the direction cosines. Assuming parallel ordering within transverse planes and antiparallel ordering between adjacent planes, we will show that classical interactions give rise to a negative axial anisotropy. A brief discussion follows on the origin of the sixfold anisotropy in the plane.

To determine the dipole field at a given Mn^{2+} site in the hexagonal structure we utilize the fact that the undistorted hexagonal structure can be obtained by two interlaced face-centered cubic (fcc) sublattices. This should give a good estimate of the dipole field at a hexagonal site because only the Mn_2 sites are displaced by 0.21 Å from the center of gravity of its octahedron.[21] The $\langle 00.1\rangle$ directions correspond to the $\langle 111\rangle$ directions

[39] K. Lee, thesis, University of California, Berkeley, 1963 (unpublished).

in the fcc structure, in which case the transverse planes correspond to {111} planes.

With ferromagnetic ordering in the planes and antiferromagnetic ordering between adjacent planes the hexagonal stacking of the Mn^{2+} sites along the ⟨00.1⟩ direction is given by

$$A(+)B(-)B(+)A(-)C(+)C(-)A(+)B(-)\cdots,$$

where A, B, and C denote the different crystallographic positions of the six Mn^{2+} ions in the unit cell and the (+) and (−) notation denotes the relative spin directions. The distance between each plane of the undistorted structure is $0.41a$, where $a=6.213$ Å is the distance between Mn sites within a plane. For one fcc lattice the ferromagnetically ordered stacking along the ⟨111⟩ direction is given by

$$A(+)B(+)C(+)A(+)B(+)\cdots,$$

where the distance between (111) planes is $(\frac{2}{3})^{1/2}a=0.82a$. Interlacing this lattice with one which has the inverted stacking along its ⟨111⟩ direction,

$$C(-)B(-)A(-)C(-)B(-)A(-)\cdots,$$

we obtain the hexagonal stacking above. The distance between (111) planes of one sublattice with (111) planes of the other is now equal to $0.41a$.

We recall that classical dipolar interactions fail to yield cubic anisotropy. The anisotropy at a given site in one of the fcc sublattices is therefore due to the array of dipoles of the other fcc sublattice. McKeehan[40] has computed the dipole fields in certain cubic arrays of equal parallel dipoles. These fields are computed for high symmetry positions. For a fcc lattice the dipole field at a $(\frac{1}{4}\frac{1}{4}\frac{1}{4})$ position is zero because of the local $\bar{4}3m$ point symmetry.

Since we are interested in the dipole field at the $(\frac{1}{6}\frac{1}{6}\frac{1}{6})$ position which corresponds to a dipole position in a (111) plane of the other fcc sublattice, we determine this field by carrying out a field expansion about the $(\frac{1}{4}\frac{1}{4}\frac{1}{4})$ position

$$H(z)=H(z_0)+(z-z_0)H_Q+\frac{(z-z_0)^2}{2}H_{0c}+\cdots, \quad (39)$$

where $\mathbf{z}$ denotes the axis in the ⟨111⟩ direction, $z=(\frac{1}{6})^{1/2}a$, $z_0=(\frac{3}{8})^{1/2}a$, $H(z_0)$ is the dipole field at z_0, and $H_Q=-\sum_{i<j}\partial H(z)/\partial z_j$ and $H_{0c}=-\sum_{i<j}\partial H_Q(z)/\partial z_j$ are, respectively, the quadrupole and octupole fields. The negative sign in H_Q and H_{0c} is introduced because we are carrying out the summation from the field position $(\frac{1}{4}\frac{1}{4}\frac{1}{4})$ to the dipole positions. From the usual expression for the dipole field, we have

$$H_Q=-3\mu\sum_{i<j}\left(\frac{1}{r_{ij}}\right)^7(3z_jr_{ij}^2-5z_j^3),$$
$$H_{0c}=3\mu\sum_{i<j}\left(\frac{1}{r_{ij}}\right)^9(3r_{ij}^4-30z_j^2r_{ij}^2+35z_j^4). \quad (40)$$

For a given fcc sublattice with all dipoles parallel to the ⟨111⟩ direction, this summation is extended to the seventh nearest neighbors. We find for the quadrupole and octupole fields

$$H_Q=-88.57\mu/a^4,$$
$$H_{0c}=+256.41\mu/a^5. \quad (41)$$

With $H(z_0=\frac{1}{4})=0$, we finally have for the dipole field at the $(\frac{1}{6}\frac{1}{6}\frac{1}{6})$ position

$$H_D(\tfrac{1}{6}\tfrac{1}{6}\tfrac{1}{6})=4530\text{ Oe}. \quad (42)$$

This is then the dipole field due to one sublattice at the position of a dipole belonging to the other sublattice. The energy of interaction is, therefore, $+\frac{1}{2}H_DM$.

We know the energy of interaction between two arrays of dipoles is just $-K_D(1-3\cos^2\theta)$, where θ is the polar angle measured from the c axis. For dipoles parallel to the transverse plane, $U_{\parallel}=-K_D$ and for dipoles perpendicular to the plane $U_{\perp}=+2K_D$. Since we have calculated $U_{\perp}=\frac{1}{2}H_DM>0$, we see that the transverse plane is a plane of minimum energy. Dipolar interactions, therefore, tend to align the spins parallel to the transverse planes.[41]

Again assuming a small displacement $\delta\theta$ out of the transverse planes, the energy is

$$U\sim 3K_D\delta\theta^2=\tfrac{1}{2}H_A^{\text{eff}}M\delta\theta^2.$$

Since $K_D=\frac{1}{4}H_DM$, the effective dipolar anisotropy field is given by

$$H_A^{\text{eff}}(\text{dipole})=\tfrac{3}{2}H_D=6795\text{ Oe}. \quad (43)$$

By summing Eqs. (38) and (43), we have for the total effective axial anisotropy field

$$H_{A,1}^{\text{eff}}=7965\text{ Oe}. \quad (44)$$

We have seen that crystalline fields and classical dipolar interactions give rise to a negative axial anisotropy. If the dipoles are treated as quantum dipoles, we expect that observed sixfold anisotropy in the transverse plane can, thus, be understood. This reasoning follows from the fact that quantum dipoles can be thought of as precessing about their classical direction or their axis of quantization. The energy of the hexagonal array of dipoles, which can be considered as two fcc arrays, depends upon the direction that axis takes with respect to the crystal axes. This was first worked out for a cubic ferromagnet by Van Vleck[42] using second-order perturbation of the dipolar interaction applied to energy levels in the Weiss molecular field. He considers the anisotropy to originate from an effective coupling energy

$$\mathcal{H}_D(\text{QM})=\sum_{i,j}D_{ij}[\mathbf{S}_i\cdot\mathbf{S}_j-3r_{ij}^{-2}(\mathbf{S}_i\cdot\mathbf{r}_{ij})(\mathbf{S}_j\cdot\mathbf{r}_{ij})]$$

[40] L. W. McKeehan, Phys. Rev. **43**, 913 (1933).

[41] J. I. Kaplan has shown [J. Chem. Phys. **22**, 1709 (1954)] that for MnO which has antiferromagnetic ordering between (111) planes, magnetic dipolar interactions with next-nearest neighbors align the spins parallel to these planes.

[42] J. H. Van Vleck, Phys. Rev. **52**, 1178 (1937).

plus a quadrupole-quadrupole coupling term, both taken between nearest neighbor spins. D_{ij} is a temperature-independent coupling constant which need not be equal to $g^2\mu_B^2/r_{ij}^3$. With the dipoles treated quantum mechanically, there are terms nondiagonal in $\sum_j S_j^z$. $\mathcal{H}_D$(QM), thus giving rise to cubic anisotropy.

Pearson[43] has considered the dipolar anisotropy in antiferromagnetic cubic lattices. He obtains the cubic anisotropy from a general spin-wave calculation of the zero-point dipole-dipole energy and finds that this anisotropy is of the same magnitude as in the ferromagnetic case.

We can determine an estimate of this in-plane anisotropy field by noting that it is approximately equal to the square of the nearest neighbor interaction energy divided by the exchange field. With d equal to the distance between nearest neighbor Mn ions, we find for this field

$$H_{A,3}\sim(g\mu_B S/d^3)^2/H_E\approx 2\text{ Oe}. \tag{45}$$

Interpretation of Results

From the experimental susceptibility and torsion results, we may conclude that $CsMnF_3$ has antiferromagnetic ordering with negative axial anisotropy. With a spin model such that the magnetizations are in the transverse plane and a critical field of 900 Oe indicated, a good estimate of the exchange field can be made from the susceptibility measurements. We see from Eq. (30) that for measurements at high fields χ_b should be larger than χ_c by 1%. We note in Fig. 2 that this is consistent with our observations. Assuming $\chi_{11}(4.2°\text{K})$ to be nearly zero such that $1/\lambda=\chi(4.2°\text{K})=39.7\times10^{-3}$ emu/mole and calculating $M=13\,850$ emu/mole, we find for the exchange field

$$H_E=\lambda M=3.5\times10^5\text{ Oe}. \tag{46}$$

The expressions for the torque for low applied fields is given by Eq. (16) and plotted in Fig. 3. The fit to the experimental data at the two lowest fields where the two- and fourfold terms dominate is quite good while the fit at the higher field where the sixfold term emerges is only fair. We believe the two and fourfold terms are due to antiferromagnetic domains while the sixfold term arises from the symmetry of the plane. Wall displacement would thus play an important role as the field is increased to 600 Oe. This wall motion would then cause a poor fit at the higher field since wall displacements were not taken into account in the theory. To determine $K_3\lambda$, which arises from the sixfold symmetry of the plane, we Fourier analyzed the 600 Oe data. We find $K_3\lambda=1.09\times10^4$ Oe^2. Using the value of λ obtained above, we find for the sixfold anisotropy field

$$H_{A,3}=36K_3/M=1.12\text{ Oe}. \tag{47}$$

This is in reasonable agreement with our estimated value of 2 Oe. We also note that Eq. (16) gives the H^2 dependence observed at low fields. With this value of $K_3\lambda$, the critical field for flopping is $H_c\simeq(72K_3\lambda)^{1/2}\simeq900$ Oe which is consistent with observations.

For the high-field results we see that Eq. (25) yields a sixfold dependence independent of the applied field. This agrees with the observations at high fields. Using the data obtained at 9000 Oe, we calculated $H_{A,3}=1.1$ Oe, which agrees with our low field results.

The high-field expression for the torque in the $\{2\bar{1}.0\}$ plane yields the observed twofold symmetry and gives us a means for determining the axial anisotropy field $H_{A,1}$. From the high-field data, we find

$$H_{A,1}=7500\text{ Oe}. \tag{48}$$

This is in satisfactory agreement with the theoretical value of 7965 Oe obtained from crystalline field and dipolar calculations.

From Eq. (25) we see that by observing the temperature dependence of the torque in the transverse plane at high fields, we are actually observing $K_3(T)$. Assuming $K_3(0)\lambda=1.09\times10^4$ Oe^2 we plot $K_3(T)/K_3(0)$ versus T^2 in Fig. 10. The field of 6 kOe is applied at 45° with respect to a ⟨12.0⟩ direction. The temperature dependences of $K_3(T)$ and $M(T)$ according to spin-wave theory are given by Eqs. (31) and (32). Since $n=6$ and

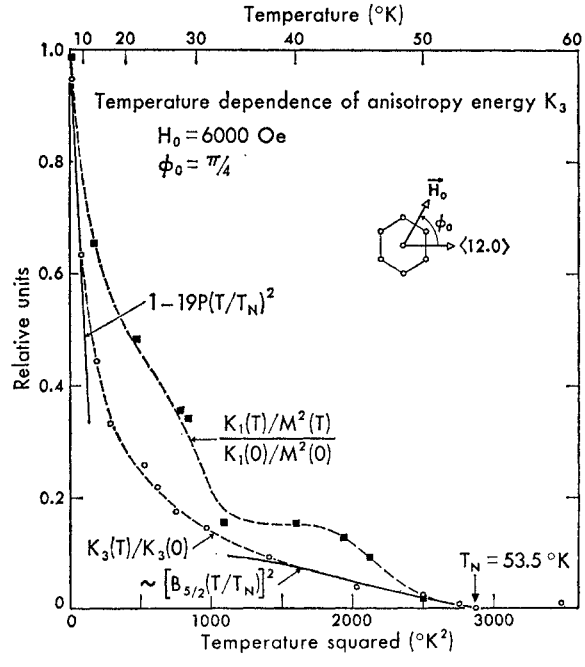

FIG. 10. Temperature dependence of the anisotropy energy K_3. The open circles are the experimental points for $K_3(T)/K_3(0)$. Also shown is the experimental temperature dependence of $K_1(T)/M^2(T)$, represented by the square points. The dashed lines are best fits to the experimental points. The dependences according to spin-wave theory and molecular field theory are indicated, respectively, by $[1-19P(T/T_N)^2]$ and $[B_{5/2}(T/T_N)]^2$ where $B_{5/2}(T/T_N)$ is the modified Brillouin function.

[43] J. J. Pearson, Phys. Rev. **121**, 695 (1961).

$m=1$, we have

$$K_3(T)/K_3(0)\approx 1-19P(T/T_N)^2 \qquad (49)$$

for $T\ll T_N$. By fitting this expression to the data, we find $P=0.64$. In Fig. 10 we see that the rapid decrease of $K_3(T)$ agrees with spin-wave theory for $T<10°K$. At high temperatures, $K_3(T)$ is proportional to the square of the sublattice magnetization given by Eq. (33). The square of the modified Brillouin function is also plotted in Fig. 10 and we see that $K_3(T)$ agrees with molecular field theory for $35°<T<T_N$. As yet, there is no satisfactory theory which would satisfy the large intermediate temperature region.

The temperature dependence of the torque in the $\{2\bar{1}.0\}$ plane gives us an experimental observation of $K_1(T)/M^2(T)$. The main contribution to K_1 is the long-range dipolar interactions. Therefore, in the spin wave region, we expect $K_1(T)\sim M^{2.9}(T)$.[44] From Eq. (29), it follows that for $H_0=6$ kOe and $\theta_0=25°$, the ratio K_1/M^2 is given by

$$\frac{K_1(T)/M^2(T)}{K_1(0)/M^2(0)}=4.3\tau(T)\times 10^{-3}. \qquad (50)$$

We also note in Fig. 10 that for $30°K<T<45°K$, the torque is independent of the temperature. This is in agreement with molecular field theory as $K_1(T)\propto M^2(T)$ and therefore τ is independent of the temperature.

From torsion and susceptibility measurements we have thus shown $CsMnF_3$ to be antiferromagnetically ordered. Because of the presence of an easy plane, we were able to determine the axial anisotropy field, which is 10^3 larger than the in-plane anisotropy. The temperature dependence of $K_1(T)/M^2(T)$ and $K_3(T)$ were also observed and the temperature region where spin-wave theory and molecular field theory are valid were shown. We now proceed to investigate the dynamical magnetic properties.

IV. ELECTRON RESONANCE MEASUREMENTS

Experimental Results

In this section we discuss the results of paramagnetic resonance in the temperature range from 298 to 63°K and of antiferromagnetic resonance in the temperature range from 0.3 to 4.2°K. Two standard X-band microwave spectrometers of the conventional magic-T design were used. One spectrometer, utilizing a rectangular reflection cavity which resonates in a TE_{101} mode, was used from 298 to 63°K and from 4.2 to 1.7°K. The two temperature ranges were obtained by pumping on liquid oxygen and liquid helium, respectively. The other, a low-temperature spectrometer (described by Ruby *et al.*[45]), was used to take data from 1.5 to 0.3°K. It utilizes a cylindrical cavity resonating in a TE_{111} mode and attains the low temperatures by adiabatic demagnetization. Because of the large signal-to-noise ratio, field modulation was not required.

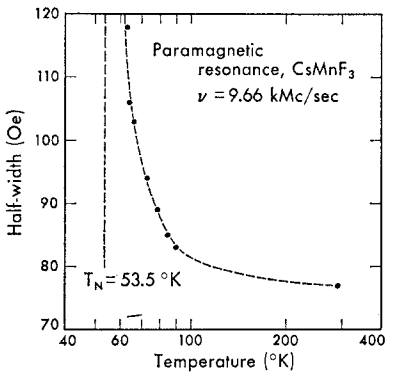

FIG. 11. Half-width of paramagnetic resonance line as a function of temperature.

Using a speck of diphenyl-picryl-hydrazyl (DPPH) with $g=2.0036$ as a marker, we observe in the paramagnetic region a single resonance line with an isotropic g value of 1.9989 ± 0.003. Considering the amount of covalent bonding observed in $KMnF_3$,[46] the deviation from the free electron g value is not unexpected. As the temperature was lowered toward the Néel point, the resonance line was observed to decrease in amplitude with a corresponding increase in the half-width at half-amplitude. This large increase, shown in Fig. 11, has been observed in other antiferromagnets such as MnF_2.[47,48] In contrast to this increase Teaney[49] observed that the linewidth and amplitude of the resonance line in $KMnF_3$ remained constant as the temperature was lowered through its Néel point. This may be related to the fact that $KMnF_3$ is nearly cubic, whereas MnF_2 and $CsMnF_3$ are highly anisotropic.

A single resonance with a half-width at half-amplitude $\Delta H_{1/2}=12\pm 3$ Oe was observed at 4.2°K. This is about as narrow a resonance line as has been observed so far in an antiferromagnet. As expected, the resonance field in the transverse plane showed a sixfold angular variation consistent with the torsion results. The resonance field was a maximum and a minimum with H_0, respectively, along the $\langle 12.0\rangle$ and $\langle 10.0\rangle$ directions. This is shown in Fig. 12, which is a plot of the angular dependence of the resonance field in the transverse plane. In another measurement the sample was strained, causing an increase of the line width to $\Delta H_{1/2}=40\pm 5$ Oe and a distortion of the sixfold symmetry. We found that the crystals could be strained quite easily by applying an excessive amount of GE-7031 varnish. A half-width of 40 Oe was not unusual for a strained sample.

Figure 13 shows the resonance field as a function of

[44] T. Oguchi, Phys. Rev. **111**, 1063 (1958).
[45] R. H. Ruby, H. Benoit, and C. D. Jefferies, Phys. Rev. **127**, 51 (1962).
[46] R. G. Shulman, K. Knox, and B. J. Wyluda, Bull. Am. Phys. Soc. 4, 166 (1959).
[47] L. R. Maxwell, Am. J. Phys. **20**, 80 (1952).
[48] L. R. Maxwell and T. R. McGuire, Rev. Mod. Phys. **25**, 279 (1953).
[49] T. Moriya, Phys. Rev. **117**, 635 (1960).

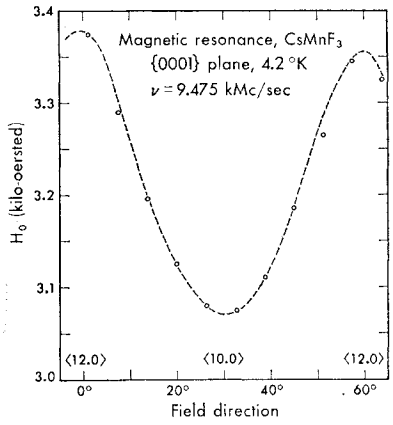

FIG. 12. Magnetic resonance in the {0001} plane at 4.2°K.

the angle Ψ in the $\{2\bar{1}.0\}$ plane. The angle Ψ is measured with respect to a $\langle 12.0\rangle$ direction. Since the resonance field is directly proportional to $(\cos\Psi)^{-1}$ only the component of the static field in the transverse plane contributes to the observed resonance. This is not surprising considering the presence of a large negative axial anisotropy energy.

Proceeding from 4.2 down to 1.7°K, the resonance line was observed to shift to a lower field position. The line width correspondingly narrowed slightly to $\Delta H_{1/2}=11\pm1$ Oe. Below 1.5°K there were as many as six lines with a peak to peak separation of the highest field and lowest field lines of only 16 Oe. At 9.6 kMc/sec the multiple lines appear at resonance fields of 3 kOe and lower. Of the six lines, there was one that was always more prominent than the others. The total half-width was 11 ± 1 Oe. These lines were definitely not observed at 4.2°K. As the temperature was lowered to 0.3°K, the lines shifted to lower field positions and decreased in amplitude with a corresponding broadening. At 0.3°K, the resonance field was well below 500 Oe. Figure 14 shows this shift in the resonance field of the most prominent line as a function of temperature. The dc field was applied along the two principal directions in the transverse plane. The square of the resonance field was found to be a linear function of $1/T$. This is shown in Fig. 15.

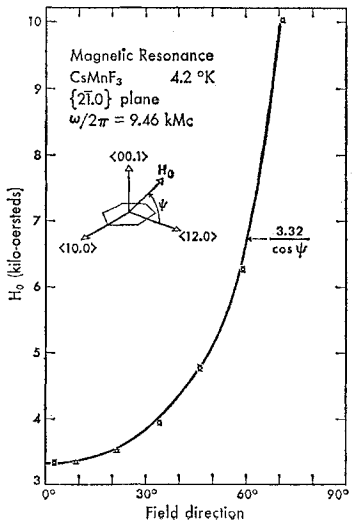

FIG. 13. Magnetic resonance in the $\{2\bar{1}.0\}$ plane at 4.2°K. The angle Ψ is the position of H_0 with respect to a $\langle 12.0\rangle$ direction.

This strong temperature dependence at liquid-helium temperatures was first observed in $KMnF_3$ by Heeger *et al.*[11,12] Heeger[11] has shown that this temperature dependence at low temperatures is the result of a strongly temperature-dependent anisotropy field seen by the electrons due to their hyperfine interaction with the Mn^{55} nuclei. Each sublattice sees this anisotropy field $H_{A,T}$ pointing along its equilibrium direction and the $1/T$ dependence originates from the nuclear susceptibility. The temperature dependence of the sixfold anisotropy in this temperature region, as given by Eq. (47), contributes very little to the observed effect.

The fact that H_0^2 is linear in $1/T$ confirms earlier observations that there does not exist a weak ferromagnetic moment. If such a moment had existed, there would be a term $H_0H_{A,C}$ in the resonance condition which is proportional to $1/T$, where $H_{A,C}$ represents the various mechanisms which would give rise to a canting of the sublattices.[11,12,49,50]

It is interesting to note that the apparent microwave cooling of the nuclei as observed in[11,12] $KMnF_3$ was not found even at the relatively low temperature of 1.8°K.

Theory of Magnetic Resonance Frequencies

From our experimental observations, we saw that in the presence of a large negative axial anisotropy, only the component of the static field in the transverse plane contributes to the resonance condition. The

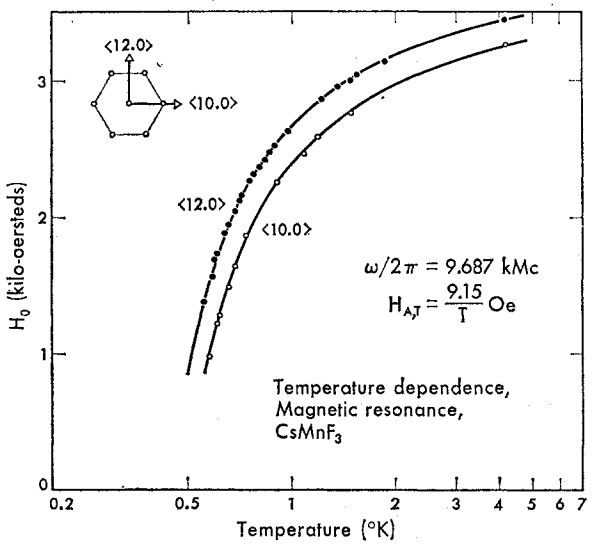

FIG. 14. Temperature dependence of the magnetic resonance field in the transverse plane. The temperature-dependent hyperfine anisotropy field is given by $H_{A,T}=9.15/T$ Oe.

[50] P. Pincus, Phys. Rev. Letters **5**, 13 (1960).

magnetic resonance frequencies will, therefore, be considered in this section with the static field confined to the transverse plane. Again the molecular field approximation for a two-sublattice antiferromagnet will be assumed. We will first derive the resonance frequencies with the static field at an arbitrary angle to a preferred or easy axis. The static field will be assumed to be much larger than the critical field for flopping. The characteristics of the normal modes are determined for $H_0=0$ and for H_0 applied perpendicular to a preferred axis. Finally, we discuss briefly the rf susceptibility.

The temperature dependent anisotropy field $H_{A,T}$ arising from the hyperfine interaction gives rise to the additional terms $-\alpha\mathbf{m}_1\cdot\mathbf{M}_1-\alpha\mathbf{m}_2\cdot\mathbf{M}_2$ in the energy where

$$H_{A,T}=\alpha m=(A/g\mu_B)\langle I_z\rangle. \tag{51}$$

$\langle I_z\rangle$ is the average nuclear spin, $\mathbf{m}_{1,2}$ are the nuclear magnetizations of the two sublattices and A is the hyperfine coupling constant. This field $H_{A,T}$ looks like an axial anisotropy field along the equilibrium direction in the transverse plane. We will initially neglect this contribution, but will include it in the final result. In a later section on the theory of electron-nuclear double resonance modes, this contribution is included explicitly.

Static Field at Arbitrary Angle in Plane

The static field H_0 is assumed to be larger than H_c and it is oriented at an arbitrary angle φ_0 in the transverse plane. Initially neglecting the hyperfine energy, the total energy is given by Eq. (1) with the angles defined in Fig. 8. Expressed explicitly in terms of the angles, the energy is

$$\begin{aligned}U=&\lambda M^2[\cos\theta_1\cos\theta_2-\sin\theta_1\sin\theta_2\cos(\varphi_1+\varphi_2)]\\&+MH_0[\sin\theta_2\cos(\varphi_0+\varphi_2)-\sin\theta_1\cos(\varphi_0-\varphi_1)]\\&-K_3[\cos6\varphi_1+\cos6\varphi_2]+\tfrac{1}{2}K_1[\cos^2\theta_1+\cos^2\theta_2].\end{aligned} \tag{52}$$

Since $K_1\gg K_3$, we neglect the perturbation out of the transverse plane due to K_3. The equilibrium conditions are just given by Eqs. (21), (22), and (23).

We now solve for the resonance frequencies following a procedure which does not require the transformation to two new coordinate systems. This procedure is quite general and considers only the small angular motions of $\mathbf{M}_1$ and $\mathbf{M}_2$. Circular precession of the magnetizations is not assumed. For small oscillations $\delta\theta_{1,2}$ and $\delta\varphi_{1,2}$ about the equilibrium positions, the angular coordinates are given by

$$\begin{aligned}\theta_{1,2}&=\tfrac{1}{2}\pi+\delta\theta_{1,2},\\\varphi_{1,2}&=\mp(\tfrac{1}{2}\pi-\Delta)+\epsilon+\delta\varphi_{1,2},\end{aligned} \tag{53}$$

where $\Delta=\varphi_0+\zeta$ and ϵ and ζ are given by the definitions (21) and (23). Substituting these relations into Eq.

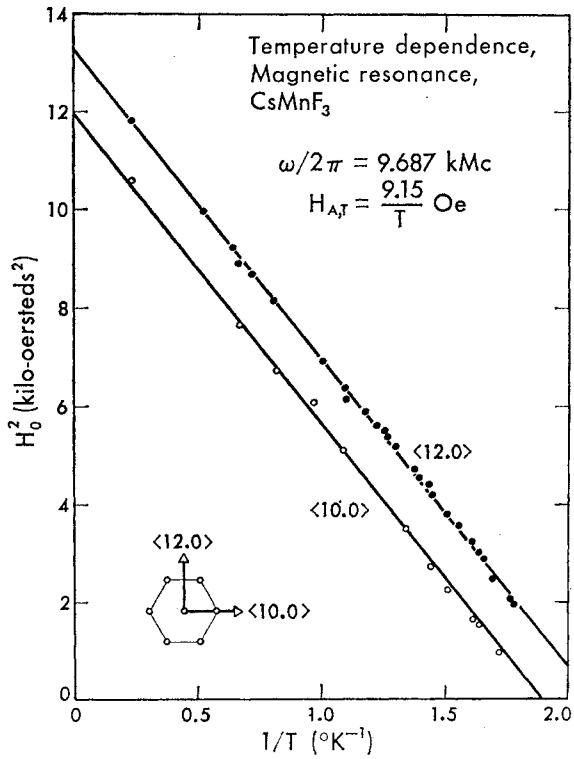

FIG. 15. Resonance field squared as a function of $1/T$.

(52), expanding to second order in $\delta\theta$ and $\delta\varphi$, we have

$$\begin{aligned}U=&\tfrac{1}{2}\delta\varphi_1^2[MH_0\sin(\zeta+\epsilon)+\lambda M^2\cos2\epsilon\\&\qquad-36K_3\cos6(\Delta+\epsilon)]\\&-\tfrac{1}{2}\delta\varphi_2^2[MH_0\sin(\zeta-\epsilon)-\lambda M^2\cos2\epsilon\\&\qquad+36K_3\cos6(\Delta-\epsilon)]\\&+\lambda M^2[\cos2\epsilon\delta\varphi_1\delta\varphi_2+\delta\theta_1\delta\theta_2]\\&+\tfrac{1}{2}\delta\theta_1^2[MH_0\sin(\zeta+\epsilon)+\lambda M^2\cos2\epsilon+K_1]\\&-\tfrac{1}{2}\delta\theta_2^2[MH_0\sin(\zeta-\epsilon)-\lambda M^2\cos2\epsilon-K_1].\end{aligned} \tag{54}$$

The coefficients of the linear terms in $\delta\varphi_1$ and $\delta\varphi_2$ vanish in the limit of strong exchange, giving the relations

$$\begin{aligned}-MH_0\cos(\zeta+\epsilon)+\lambda M^2\sin2\epsilon-6K_3\sin6(\Delta+\epsilon)\equiv0,\\-MH_0\cos(\zeta-\epsilon)+\lambda M^2\sin2\epsilon+6K_3\sin6(\Delta-\epsilon)\equiv0.\end{aligned} \tag{55}$$

These relations just give the equilibrium conditions obtained earlier. To a good approximation, the equations of motion are

$$\begin{aligned}\frac{\partial\delta\varphi_{1,2}}{\partial t}&=\mp\frac{\gamma}{M}\frac{\partial U}{\partial\delta\theta_{1,2}},\\\frac{\partial\delta\theta_{1,2}}{\partial t}&=\pm\frac{\gamma}{M}\frac{\partial U}{\partial\delta\theta_{1,2}}.\end{aligned} \tag{56}$$

Assuming an $\exp(i\omega t)$ dependence we have the usual four by four secular determinant. Expanding the terms

to second order in ϵ, we obtain

$$(\omega/\gamma)^2 \simeq \tfrac{1}{2}H_0^2(1+\sin^2\zeta) - H_E H_{A,3}\cos 6\Delta + H_E H_{A,1} \pm [H_E H_{A,1} - \tfrac{1}{2}H_0^2(5\sin^2\zeta - 1) - H_E H_{A,3}\cos 6\Delta]. \quad (57)$$

With ζ given by Eq. (21) and $\Delta = \varphi_0 + \zeta$, the two resonance frequencies are

$$(\omega_1/\gamma)^2 = H_0^2 - 2H_E H_{A,3}\cos 6\varphi_0$$

and

$$(\omega_2/\gamma) = 2H_E H_{A,1}.$$

Since the hyperfine field looks like an axial anisotropy field its effect on the resonance condition for an antiferromagnet is $2H_E H_{A,T}$,[51,52] where $H_{A,T}$ is given by Eq. (51) and $H_E \gg H_{A,T}$. Therefore, we finally have for the two modes

$$(\omega_1/\gamma)^2 = H_0^2 - 2H_E H_{A,3}\cos 6\varphi_0 + 2H_E H_{A,T} \quad (58)$$

and

$$(\omega_2/\gamma)^2 = 2H_E H_{A,1} + 2H_E H_{A,T}, \quad (59)$$

where the positive sign in the hyperfine term arises from the fact that the coupling energy αmM is a minimum along the equilibrium directions. With $H_0 \sim 10^3$, $2H_E \sim 10^6$, $H_{A,3} \sim 1$, $H_{A,1} \sim 10^4$ and $H_{A,T} \sim 1$ at 4.2°K, we see that ω_1 corresponds to the low-frequency mode which we observe at X-band and ω_2 corresponds to the high-frequency mode.

Normal Modes and rf Susceptibility

Now we consider the characteristics of the normal modes with $H_0 = 0$ and with H_0 applied perpendicular to a preferred axis. The normal modes are determined by finding the ratios of the angular displacements $\delta\varphi_1/\delta\varphi_2$, $\delta\theta_1/\delta\theta_2$, $\delta\theta_1/\delta\varphi_1$, and $\delta\theta_2/\delta\varphi_2$ from the secular determinant. For the first case where $H_0 = 0$, the ratios for the low-frequency mode, ω_1, are found to be

$$\begin{aligned} \delta\varphi_1/\delta\varphi_2 &= -\delta\theta_1/\delta\theta_2 = -1, \\ \delta\theta_1/\delta\varphi_1 &= -\delta\theta_2/\delta\varphi_2 = -i\rho(0), \end{aligned} \quad (60)$$

where $\rho(0) = (H_{A,3}/2H_E)^{1/2}$ and the ratios for the high-frequency mode, ω_2, are found to be

$$\begin{aligned} \delta\varphi_1/\delta\varphi_2 &= -\delta\theta_1/\delta\theta_2 = +1, \\ \delta\theta_1/\delta\varphi_1 &= -\delta\theta_2/\delta\varphi_2 = +i\beta(0), \end{aligned} \quad (61)$$

where $\beta(0) = (2H_E + H_{A,3})/(2H_E H_{A,1})^{1/2}$. For $2H_E \sim 10^6$, $H_{A,1} \sim 10^4$, and $H_{A,3} \sim 1$, these ratios are $\rho(0) \sim 10^{-3}$ and $\beta(0) \sim 10$. The (0) notation designates this case where $H_0 = 0$. $\rho(0)$ and $\beta(0)$ are just the eccentricities of the elliptical orbits described by the motion of the magnetizations. The characteristics of the normal modes are, therefore, determined from Fig. 8 and these ratios and these modes are shown in Fig. 16(a).

For the low-frequency mode, the magnetization vectors $\mathbf{M}_1$ and $\mathbf{M}_2$ precess at frequencies $\omega_1(0)$ counter-

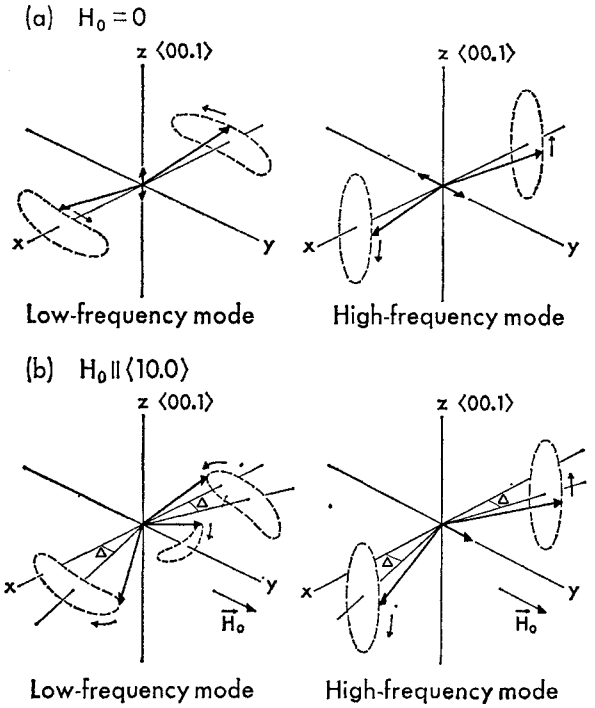

FIG. 16. Normal modes (a) with $H_0 = 0$ and (b) with $\mathbf{H}_0$ applied along a ⟨10.0⟩ direction. The angle Δ is given by equation (7) with $\varphi_0 = \Phi = \frac{1}{2}\pi$.

clockwise (or clockwise) about their respective equilibrium directions and they are out of phase by π. They describe equal size ellipses with the ratio of minor to major axes equal to $\rho(0)$. There is a small net oscillating moment in the z direction.

For the high frequency mode, the magnetization vectors precess counterclockwise (or clockwise) at frequency $\omega_2(0)$ about their respective equilibrium directions, but they are in phase. They describe equal size ellipses with the ratio of major to minor axes equal to $\beta(0)$. There is a net oscillating moment in the y direction.

From Fig. 16(a), we see that the rf susceptibility can be determined quite simply from the Kramers-Kronig relations. It can be shown that $\chi''(\omega_0) = (\chi_0\omega_0/2\Delta\omega_1)$, where χ'' is the imaginary part of the rf susceptibility, ω_0 is the resonance frequency, χ_0 is the static susceptibility, and $\Delta\omega_1$ is the half-width at half-intensity. Therefore, for the low-frequency mode, with an rf field H_1 parallel to the z axis,

$$\chi''(\omega_1) = \tfrac{1}{2}\chi_c(\omega_1/\Delta\omega_1); \quad (62)$$

and for the high-frequency mode, with H_1 parallel to the y axis,

$$\chi''(\omega_2) = \tfrac{1}{2}\chi_{1c}(\omega_2/\Delta\omega_2), \quad (63)$$

where χ_c and χ_{1c} are the static susceptibilities parallel and perpendicular to the c axis.

Let us now consider H_0 applied perpendicular to the

[51] C. Kittel, Phys. Rev. **82**, 565 (1951).
[52] F. Keffer and C. Kittel, Phys. Rev. **85**, 329 (1952).

preferred direction. The equilibrium positions of the two sublattices are canted toward the field by an angle Δ given by Eq. (7) with $\varphi_0=\Phi=\frac{1}{2}\pi$. The resonance frequencies are given by Eqs. (58) and (59) with $\varphi_0=\frac{1}{2}\pi$. The ratios of the angular displacements have exactly the same form as Eqs. (60) and (61) except that the eccentricities of the orbits are changed. In this case we have

$$\rho=\frac{(H_0^2+2H_EH_{A,3})^{1/2}}{2H_E},$$
$$\beta=\frac{(2H_E^2-\frac{1}{2}H_0^2+H_EH_{A,3})}{(2H_E^3H_{A,1})^{1/2}}, \tag{64}$$

where $\rho\sim10^{-3}$, $\beta\sim10$ for $H_0\sim3\times10^3$. The relative phases are not changed.

However, as shown in Fig. 16(b), the net oscillating moments for the low- and high-frequency modes are different from those in zero field. In the low-frequency mode the magnetizations swing back and forth in phase such that the net moment oscillates elliptically in essentially the xy plane. Because of the large eccentricity ($\sim10^{-3}$) we may assume that the moment is only rocking in the transverse plane. In the high-frequency mode the net oscillating moment is always pointing along H_0. This is just due to the motion of the magnetizations being in phase.

Interpretation of Results

The broadening of the paramagnetic resonance line with a corresponding reduction in the absorption as the Néel temperature is approached is characteristic of all noncubic antiferromagnets. Maxwell and McGuire[47,48] have earlier reported such observations. Tsuya and Ichikawa[53] derived an equation for the linewidth as the temperature approaches the Néel point. However, they neglect any anisotropy energy that exists and their result is valid only for simple cubic and body-centered cubic structures. As yet we know of no satisfactory general theory explaining these observations.

It is of interest to compare our observations with Anderson and Weiss' prediction for the exchange narrowed dipolar linewidth.[54] They derive the general relation for the half-width at half-power

$$\Delta H_{1/2}=H_p^2/H_E,$$

where

$$H_p^2=(5.1)(g\mu_BN)^2S(S+1),$$
$$H_E=2.83(J/g\mu_B)[S(S+1)]^{1/2},$$

J is just the exchange integral, $S=\frac{5}{2}$, and N is the density of spins per cm^3. Using the usual molecular field relations for J [36,54] and the value of the measured susceptibility $\chi_1=\chi(T_N)$, we find $\Delta H_{1/2}\approx50$ Oe, compared to the observed value $\Delta H_{1/2}(298°\text{K})\approx75$ Oe. Considering the approximations that were made in obtaining the above relation, the comparison is fairly good.

At liquid-helium temperatures, it is obvious we are observing the low-frequency mode, ω_1. Equation (58) not only satisfies the observed sixfold symmetry, but by comparing with the experimental observations it shows the $\langle12.0\rangle$ directions to be the easy directions. We can also determine $H_{A,3}$ by the relation

$$H_{A,3}=\frac{H_0(\Delta H_0/\Delta\varphi_0)}{6H_E\sin6\varphi_0}. \tag{65}$$

With $H_E\sim3.5\times10^5$ Oe and data such as that plotted in Fig. 12, we calculate $H_{A,3}\simeq1$ Oe. These results are consistent with our static measurements.

To determine $H_{A,T}$, we assume $H_{A,3}=1.1$ Oe, and fit the experimental data shown in Fig. 15 to Eq. (58). We find

$$H_{A,T}=9.15/T\text{ Oe}. \tag{66}$$

This is compared to the values of $9.7/T$ Oe observed in $KMnF_3$ [11,12] and $9.43/T$ Oe calculated for $RbMnF_3$.[17]

The reason for the single resonance line degenerating into at least six lines at temperatures below 1.5°K is understood as due to the resonance field being close to the critical field for flopping. These lines may then arise from individual domains. To obtain a better understanding of these lines, lower frequency (3–6 kMc/sec) measurements should be made.

From torsion measurements, we measured $H_{A,1}=7500$ Oe. The high-resonance mode given by Eq. (59) should, therefore, occur in the liquid-helium temperature region at $\omega/2\pi\simeq200$ kMc/sec or 1.5 mm.

V. NUCLEAR-ANTIFERROMAGNETIC DOUBLE RESONANCE

The strong temperature dependence of the antiferromagnetic resonance field in the liquid-helium temperature range, as shown in Figs. 14 and 15, provides a means for observing the Mn^{55} nuclear resonance. With the dominant hyperfine interaction proportional to the nuclear magnetization, it is possible to observe the nuclear resonance absorption by monitoring the antiferromagnetic resonance field at a fixed microwave frequency. By supplying rf power at the nuclear resonance frequency to saturate the nuclear magnetization, a shift of the antiferromagnetic resonance to its high-temperature position is expected. Relevant theory by deGennes *et al.*[55] gives the expressions for the frequency ω_N of the nuclear modes in a ferro- and antiferromagnet.

[53] N. Tsuya and Y. Ichikawa, Phys. Rev. **83**, 1065 (1951).
[54] P. W. Anderson and P. R. Weiss, Rev. Mod. Phys. **25**, 269 (1953).
[55] P. G. de Gennes, F. Hartmann-Boutron, and P. A. Pincus, Compt. Rend. **254**, 1264 (1962); P. Pincus, P. G. de Gennes, F. Hartmann-Boutron, and J. M. Winter, J. Appl. Phys. **34**, S (1963); P. G. de Gennes, P. A. Pincus, F. Hartmann-Boutron, and J. M. Winter, Phys. Rev. **129**, 1105 (1963).

This theory predicts that at a given temperature T, there is a characteristic $\omega_N(T)$ and it should be possible to partially saturate the nuclei. However, Heeger *et al.*,[12,15] Portis *et al.*[16] and Witt and Portis[14] have observed in $KMnF_3$ that at a given T and above a threshold rf field, H_{rf}, the nuclear modes can be excited at any driving frequency between $\omega_N(T)$ and $\gamma_N H_N = \gamma_N \alpha M$. The unexpected behavior is explained by a spatial variation in nuclear frequency as the result of electronic pinning.[16] The regions resonating at the driving frequency can then grow at the expense of those regions resonant at $\omega_N(T)$. In this section, we report on the double- (nuclear-antiferromagnetic) resonance measurements in $CsMnF_3$. We also determine the hyperfine field $A\langle S\rangle$ for the two Mn^{55} sites and derive the macroscopic equations for the nuclear-electron spin system coupled by the hyperfine interaction.

Experimental Results

A 1-mm size crystal is mounted at the center of a small single loop rf coil which is mounted flush to the side of the rectangular cavity used earlier. According to the normal modes, an enhancement to the rf susceptibility is obtained with the microwave field H_1 perpendicular to the static field H_0 in the transverse plane. It would be advantageous then to have the rf field H_{rf} also in the plane. However, due to the geometry of the cavity, H_{rf} is always perpendicular to H_1. We, therefore, mounted the sample on a 45° polystyrene wedge such that the transverse plane was at a 45° angle with respect to H_1 and H_{rf}. H_0 was applied in the plane along a ⟨10.0⟩ direction.

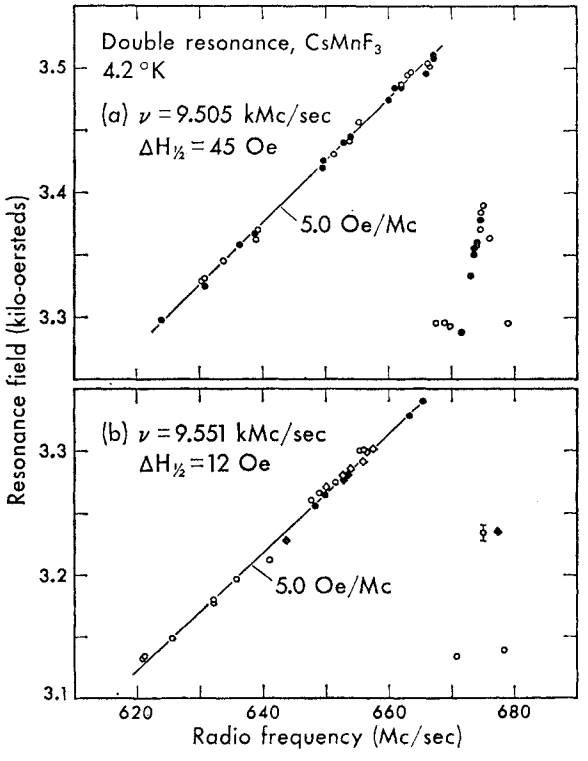

FIG. 17. Antiferromagnetic resonance field at 4.2°K as a function of radio frequency for a (a) strained and (b) unstrained sample. H_0 is parallel to a ⟨10.0⟩ direction.

A sample strained ($\Delta H_{1/2} = 43 \pm 2$ Oe) with excessive GE-7031 varnish and an unstrained sample ($\Delta H_{1/2} = 11 \pm 2$ Oe) were used. Figures 17(a) and 17(b) show the antiferromagnetic resonance field position as a function of the applied rf frequency. With no rf excitation, the resonance field positions for the strained and unstrained samples were 3.29 and 3.12 kOe, respectively. The resonance field was observed to shift to a higher field position corresponding to a high-nuclear temperature. In the case of the strained sample, a total shift of ~220 Oe was observed from 624 to 668 Mc/sec (region I). A discontinuous drop to the zero rf position occurs at 668 Mc/sec which indicates a saturation of the nuclei. However, another region (II) where the line shifts by ~80 Oe occurs from 671 to 677 Mc/sec. In the case of the unstrained sample, the same effect is observed in the two regions except that it was exceedingly more difficult to shift the resonance field above 665 Mc/sec. This is compatible with the theory of spatial variation in nuclear frequency due to electronic pinning in the region of volume imperfections and strains. The electron resonance positions above 668 Mc/sec are shifted slightly to higher fields due to heating. In both regions, as the rf power is increased, the high-field line was observed to grow at the expense of the low-field line. At intermediate rf power levels there is a partial shift such that the high- and low-field lines are simultaneously present. Both field positions are independent of power. This emergence of the line at a definite higher field position was observed also in $KMnF_3$.[14-16] In both samples, we observed that as the driving frequency approached higher frequencies, more power was required to shift the line to its high-field position. This is consistent with theory.[16] We also note that the data within region I falls on a straight line which has a slope of 5.0 Oe/Mc/sec.

Hyperfine Field and Nuclear Magnetic Resonance Modes

The hyperfine field $A\langle S\rangle$ is determined for the two Mn^{55} sites by making corrections for the volume of the distorted F^- octahedrons. Ogawa[56] has determined the fluorine volume dependence of A from paramagnetic resonance measurements of Mn^{2+} in $KMgF_3$, $KCaF_3$, and K_2MgF_4 by plotting A versus $(Mn-F)^3$, where $Mn-F$ is the bonding distance. We can obtain a good estimate of $A(Mn_1)$ and $A(Mn_2)$ from a plot of Ogawa's data. With $V(Mn_1-F_2) = 12.67$ Å^3 and $V(Mn_2-F_2, Mn_2-F_1) = 12.05$ Å^3 we find $A(Mn_1) = (92.3 \pm 0.9) \times 10^{-4}$ cm^{-1} and $A(Mn_2) = (91.9 \pm 0.9) \times 10^{-4}$ cm^{-1}.

[56] S. Ogawa, J. Phys. Soc. Japan **15**, 1475 (1960).

Neglecting zero-point excitation such that $\langle S\rangle=\frac{5}{2}$, we have

$$A(\mathrm{Mn}_1)\langle S\rangle/h=692\pm7\ \mathrm{Mc/sec} \tag{67}$$

and

$$A(\mathrm{Mn}_2)\langle S\rangle/h=688\pm7\ \mathrm{Mc/sec}. \tag{68}$$

We will show that the nuclear resonance frequency is directly proportional to $\gamma_N\alpha M$, where αM is the hyperfine field at the nucleus and γ_N is the nuclear magnetomechanical ratio. Since the Mn_1 and Mn_2 sites are equal to one third and two thirds, respectively, of the total Mn^{2+} sites, we have for an average saturation magnetization frequency

$$\langle\gamma_N\alpha M_0\rangle/2\pi=689\pm7\ \mathrm{Mc/sec}. \tag{69}$$

We now derive the nuclear resonance frequencies for the coupled nuclear-electron spin system. An average hyperfine field $\gamma_N\alpha M$ which does not make a distinction between the two Mn^{2+} sites will be assumed. To simplify the algebra, $H_0(\gg H_c)$ is again oriented perpendicular to the preferred axis in the transverse plane. With $\mathbf{m}_1(\theta_3,\varphi_3)$ and $\mathbf{m}_2(\theta_4,\varphi_4)$ denoting two sublattices and $|\mathbf{m}_1|=|\mathbf{m}_2|$, the total energy is given by Eq. (52) plus the additional terms

$$\begin{aligned}-mH_0[&\sin\theta_3\sin\varphi_3+\sin\theta_4\sin\varphi_4]\\&-\alpha mM[\sin\theta_1\sin\theta_3\cos(\varphi_1-\varphi_3)\\&+\sin\theta_2\sin\theta_4\cos(\varphi_2-\varphi_4)\\&+\cos\theta_1\cos\theta_3+\cos\theta_2\cos\theta_4],\end{aligned} \tag{70}$$

where θ_1, θ_2, φ_1, and φ_2 are defined in Fig. 8, θ_3 and θ_4 are the polar angles measured from the z axis and φ_3 and φ_4 are the azimuthal angles measured, respectively, from the $+x$ and $-x$ axis. To determine the equilibrium positions, we let $\theta_1=\theta_2=\frac{1}{2}\pi=\theta_3=\theta_4$, $\varphi_1=\varphi_2=\epsilon$, $\varphi_3=\varphi_4=\Omega$, and set $\partial U/\partial\epsilon=0=\partial U/\partial\Omega$. With $H_{A,T}=\alpha m$ and $H_N=\alpha M$, we find

$$\epsilon=\frac{H_0(1-(m/M))}{2H_E+2H_{A,T}+H_{A,3}},\quad\text{and}\quad\Omega=\epsilon+H_0/H_N.$$

Since at 4.2°K, $H_E\gg H_{A,T}+H_{A,3}$ and $m/M\ll1$, we have

$$\epsilon\simeq H_0/2H_E,\quad\text{and}\quad\Omega\simeq H_0((1/2H_E)+(1/H_N)). \tag{71}$$

Just as before we assume small angular motions of $\mathbf{M}_1$, $\mathbf{m}_1$, $\mathbf{M}_2$, and $\mathbf{m}_2$ such that

$$\begin{aligned}\theta_i&=\tfrac{1}{2}\pi+\delta\theta_i,\quad i=1,2,3,4\\\varphi_{1,2}&=\epsilon+\delta\varphi_{1,2},\\\varphi_{3,4}&=\Omega+\delta\varphi_{3,4}.\end{aligned} \tag{72}$$

Substituting into Eqs. (52) and (70) and expanding to second order in $\delta\theta$, $\delta\varphi$, we have for ϵ and Ω small

$$\begin{aligned}U\simeq&\tfrac{1}{2}(M/\gamma)A(\delta\varphi_1^2+\delta\varphi_2^2)+\tfrac{1}{2}(M/\gamma)B(\delta\theta_1^2+\delta\theta_2^2)\\&+(M/\gamma)C(\delta\varphi_1\delta\varphi_2+\delta\theta_1\delta\theta_2)\\&+\tfrac{1}{2}(m/\gamma_N)D(\delta\varphi_3^2+\delta\varphi_4^2+\delta\theta_3^2+\delta\theta_4^2)\\&-(m/\gamma_N)E(\delta\varphi_1\delta\varphi_3+\delta\varphi_2\delta\varphi_4+\delta\theta_1\delta\theta_3+\delta\theta_2\delta\theta_4),\end{aligned} \tag{73}$$

where

$$\begin{aligned}A&=\gamma(H_0\epsilon+H_E+H_{A,3}+H_{A,T}),\\B&=\gamma(H_0\epsilon+H_E+H_{A,1}+H_{A,T}),\\C&=\gamma H_E,\\D&=\gamma_N(H_0\Omega+H_N),\\E&=\gamma_N H_N.\end{aligned} \tag{74}$$

And according to the equilibrium conditions the coefficients of the linear terms vanish. Since we are only interested in solving the nuclear equations of motion, we assume the electron resonance conditions (58) and (59). At these relatively low nuclear frequencies, the electrons follow adiabatically the fields given by A/γ and B/γ. Therefore, we determine the displacements of the sublattice magnetizations as a function of the displacements of the nuclear magnetization by setting $\partial U/\partial\delta\varphi_{1,2}=\partial U/\partial\delta\theta_{1,2}=0$. The displacements are

$$\begin{aligned}\delta\varphi_{1,2}&=(\gamma\alpha m/\omega_1^2)(A\delta\varphi_{3,4}-C\delta\varphi_{4,3}),\\\delta\theta_{1,2}&=(\gamma\alpha m/\omega_2^2)(B\delta\theta_{3,4}-C\delta\theta_{4,3}),\end{aligned} \tag{75}$$

where ω_1^2 and ω_2^2 are the electron resonance frequencies. After substituting Eqs. (75) into expression (73) for the energy we determine the equations of motion to a good approximation by

$$\begin{aligned}\partial\delta\varphi_{3,4}/\partial t&=\mp(\gamma_N/m)(\partial U/\partial\delta\theta_{3,4}),\\\partial\delta\theta_{3,4}/\partial t&=\pm(\gamma_N/m)(\partial U/\partial\delta\varphi_{3,4}).\end{aligned} \tag{76}$$

On solving the secular determinant, we find for the nuclear resonance frequencies

$$(\omega_{N,1}/\gamma_N)^2=H_N^2[1-(\omega_0/\omega_1)^2], \tag{77}$$

$$(\omega_{N,2}/\gamma_N)^2=H_N^2[1-(\omega_0/\omega_2)^2], \tag{78}$$

where $(\omega_0/\gamma)^2=2\lambda M\alpha m$ would be the antiferromagnetic resonance frequency in the hyperfine anisotropy field alone and $\gamma_N H_N$ is the saturated nuclear resonance frequency. The nuclear resonance frequency squared is, therefore, depressed by an amount proportional to the nuclear magnetization. We see also that even with no external field the nuclear resonance frequencies are split where the low- and high-frequency nuclear modes correspond respectively to the low- and high-frequency electron modes. This splitting is due to the presence of a weak sixfold anisotropy in an easy plane (large negative axial anisotropy) which gives rise to elliptical precession of the electron resonance modes. These two nuclear modes are exactly analogous to the two nuclear modes for a canted antiferromagnet.[15,16,57]

From the secular determinant, we determine the relative amplitudes of the two nuclear modes. For the low-frequency nuclear mode, $\omega_{N,1}$, $\delta\varphi_3/\delta\varphi_4=-1$, $\delta\theta_3/\delta\theta_4=+1$ and for the high-frequency mode, $\omega_{N,2}$, $\delta\varphi_3/\delta\varphi_4=+1$, $\delta\theta_3/\delta\theta_4=-1$. Corresponding to the low-frequency electron mode where $\mathbf{M}_1$ and $\mathbf{M}_2$ rock

[57] A. M. Portis, G. L. Witt, and A. J. Heeger (to be published).

together in the transverse plane [Fig. 16(b)], the low-frequency nuclear mode represents also a rocking together of $\mathbf{m}_1$ and $\mathbf{m}_2$ in the plane. This rocking of the nuclear magnetizations in the plane is therefore being driven by the low-frequency mode of the electrons. For the high-frequency mode $\mathbf{m}_1$ and $\mathbf{m}_2$ oscillate π out of phase and perpendicular to the transverse plane. Let us now consider the enhancement factor relating the effective rf field seen by the nuclei to the applied rf field, H_x.[58] With H_x applied along the preferred axis perpendicular to H_0, it can be shown quite easily that the enhancement factor is given by

$$\eta \simeq 4(\omega_0/\omega_{1,2})^2(M/m)(H_0/H_E). \quad (79)$$

For the low-frequency mode, $\eta \sim 10^3$, and for the high-frequency mode, which was shown earlier to be in the far-infrared, $\eta \sim 1$. Therefore, in the presence of the low-frequency mode, it is difficult to observe the high-frequency mode. In fact we see from the normal modes that the excitation of the high-frequency mode occurs when the rf field is parallel to the dc field.

An estimate of the amount of frequency depression for the low-frequency mode at 4.2°K is given by

$$|\delta\omega_{N,1}/\omega_{N,1}| \sim (\gamma^2 \lambda M \alpha m/\omega_1^2) \sim 0.3,$$

which is relatively large.

Interpretation of Results

The partial shift of the antiferromagnetic resonance as a function of rf power is due to the partial saturation of the nuclei. The extent of the saturation is sufficient to shift the nuclear resonance up to the driving frequency. Driving at $\gamma_N \alpha M$ fully saturates the nuclear magnetization and gives rise to the maximum possible shift in the antiferromagnetic resonance. Reducing the driving frequency reduces the amount of saturation and the antiferromagnetic resonance field drops accordingly.

Since we have derived the nuclear resonance modes assuming an average hyperfine field, the above results should be valid for nuclear driving frequencies up to the calculated average saturation at $\langle \gamma_N \alpha M_0 \rangle / 2\pi = 689 \pm 7$ Mc/sec. However, we observe a saturation at 668 Mc/sec which is $(3 \pm 1)\%$ smaller than the expected value. This indicates the presence of a zero-point reduction in the electron spin $\langle S \rangle$ expected from spin-wave calculations by Anderson[31] and Kubo[33] and from calculations involving linked-spin-cluster expansions by Davis.[59] With four nearest neighbors and $S = \frac{5}{2}$, as for the Mn_2 sites in this compound, spin-wave theory and Davis' perturbation expansion predict, respectively, a 7.88 and a 4.36% reduction in $\langle S \rangle$. The observed reduction is in reasonable agreement with the two expected values.

[58] A. M. Portis and A. C. Gossard, Suppl. J. Appl. Phys. **31**, 205 S (1960).

[59] H. L. Davis, Phys. Rev. **120**, 789 (1960).

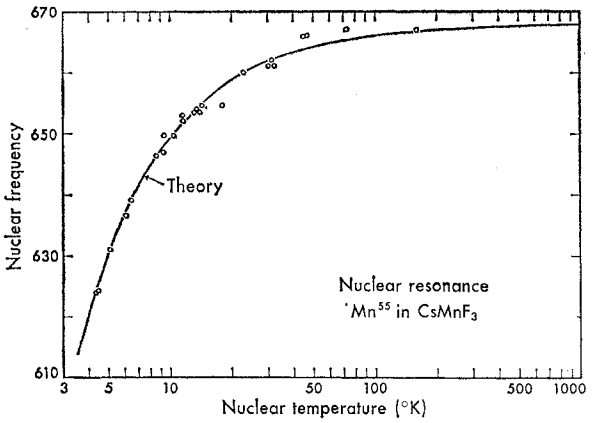

FIG. 18. Mn^{55} nuclear resonance frequency versus nuclear temperature.

It is interesting to note that in $KMnF_3$, with six nearest neighbors, there was at best a $(0.5 \pm 1)\%$ observed reduction.[15,16] Spin-wave theory and Davis' calculations predict, respectively, a 3.12 and 2.49% reduction. The zero-point excitation is, therefore, more easily observed in materials with fewer nearest neighbors which is in agreement with the two theories.

The results above 668 Mc/sec are not well understood. The observed effects may be due to regions of smaller zero-point excitation. More extensive experimental measurements and theoretical study are needed. Our discussion is, therefore, restricted to region I.

Combining Eqs. (58) and (77) for the low-freqeuncy electron and nuclear modes, we find $H_0/\nu_N = (\omega_1/\gamma\gamma_N H_N) = 5.1$ Oe/Mc/sec for $\gamma_N H_N/2\pi = 668$ Mc/sec. This is in agreement with observations.

From a comparison of the observed rf frequency-resonance field relation with the observed temperature dependence of the antiferromagnetic resonance field (Fig. 14), we can determine the temperature dependence of the nuclear resonance frequency. Figure 18 shows a plot of the nuclear resonance frequency (the driving frequency) as a function of the extrapolated nuclear temperature. The data are those of the strained sample. The observed reduction in nuclear resonance frequency with decreasing nuclear temperature is in excellent agreement with theory. The frequency extrapolated to high temperatures appears to be 668 Mc/sec which is in accordance with a 3% zero-point reduction in the electron spin.

SUMMARY

Whereas $KMnF_3$ is a canted antiferromagnet and $RbMnF_3$ is a simple cubic antiferromagnet at low temperatures, we have shown from static and dynamical magnetic measurements that below 53.5°K $CsMnF_3$ is a hexagonal antiferromagnet with a large negative axial anisotropy. Throughout our investigation we have assumed a two-sublattice model, a space group $P6_3/mmc$

at low temperatures and a magnetic unit cell identical to the chemical unit cell. From the measurement of an average perpendicular susceptibility at 4.2°K, an exchange field $H_E=3.5\times10^5$ Oe was determined. From torsion measurements we determined in the transverse plane a critical field $H_c\simeq900$ Oe and a sixfold anisotropy $H_{A,3}=1.1$ Oe and along the c axis the axial anisotropy $H_{A,1}=-7500$ Oe.

Assuming a magnetic spin model with the sublattice magnetizations lying in the transverse plane, low- and high-field expressions for the torque were determined and were found to be consistent with experimental observations. The ⟨12.0⟩ directions were established to be the preferred axes. A calculation of the ligand field anisotropy arising from the displacement of the nearest neighbor fluorines and a calculation of the classical dipolar interactions show a combined axial anisotropy of −7965 Oe. The sixfold anisotropy K_3 arising from second order dipolar interactions was estimated to be ≈2 Oe. The two calculated anisotropy fields are in reasonable agreement with the torque and resonance measurements.

The temperature dependence of K_3 was observed from 4.2° to the transition temperature and the regions where spin-wave theory and molecular field theory appear to be valid are shown in Fig. 10. We have found that K_1/M^2 decreases much more rapidly with increasing temperature than expected from spin-wave theory and also that it is constant over a high-temperature region in agreement with molecular field theory.

Paramagnetic resonance measurements show a decreasing absorption and increasing linewidth as the temperature is lowered from 298 to 63°K. This effect was also observed in other noncubic antiferromagnets. An isotropic g value of 1.9989 ± 0.003 was determined in this region. Magnetic resonance measurements at 4.2°K show a sixfold anisotropy consistent with the torsion measurements. A half-width at half-amplitude of 12 ± 3 Oe is observed which is about as narrow a resonance line as has been observed for an antiferromagnet. Due to the presence of the easy plane, we observed the resonance out of the plane to be due only to the component of the static field in the plane. From 4.2 to 0.3°K a large temperature-dependent shift in the low-frequency antiferromagnetic mode exists as expected. This shift is due to the temperature dependent hyperfine anisotropy field αm determined to be equal to $9.15/T$ Oe.

The two antiferromagnetic resonance frequencies were derived with H_0 in the plane and the normal modes and rf susceptibility were discussed for the case where H_0 is applied perpendicular to the preferred axis. The results are in agreement with observations.

The strong coupling between the nuclei and electrons afforded an opportunity to observe the Mn^{55} nuclear resonance indirectly by monitoring the position of the electron resonance field. There exist two regions in which we could shift the electron-resonance line. In the first region a saturation of the nuclear magnetization occurs at 668 Mc/sec which is $(3\pm1)\%$ lower than the calculated average hyperfine field of 689 ± 7 Mc/sec. This suggests the presence of zero-point reduction in electron spin expected from spin-wave theory. Expressions for the frequencies of the two nuclear modes were derived and it was shown that the low-frequency mode is dominant as expected. The observed reduction in the nuclear resonance frequency with decreasing temperature is in excellent agreement with theory.

ACKNOWLEDGMENTS

We would like to express our gratitude to Professor A. J. Heeger for many enlightening discussions. The authors are indebted to Dr. E. Catalano for his many helpful suggestions concerning the preparation of the single crystals and Dr. A. Zalkin and Professor D. H. Templeton for their interest in the crystal structure. Thanks are also due to N Ford for his help in taking the low-temperature resonance data.